Sonoprinting liposomes on tumor spheroids by microbubbles and ultrasound

S. Roovers[1,2], J. Deprez[1,2], D. Priwitaningrum[3], G. Lajoinie[4], N. Rivron[5], H. Declercq[2,6], O. De Wever[2,7], E. Stride[8], S. Le Gac[9], M. Versluis[4], J. Prakash[3], S.C. De Smedt[1,2*], I. Lentacker[1,2*]

[1]Laboratory of General Biochemistry and Physical Pharmacy, Ghent Research Group on Nanomedicine, Ghent University, Ghent, Belgium

[2]Cancer Research Institute Ghent (CRIG), Ghent, Belgium

[3]Targeted Therapeutics, Department of Biomaterials Science and Technology, MESA+ Institute for Nanotechnology and Technical Medical (TechMed) Center, University of Twente, Enschede, The Netherlands

[4]Physics of Fluids Group, MESA+ Institute for Nanotechnology and Technical Medical (TechMed) Center, University of Twente, Enschede, The Netherlands

[5]Institute of Molecular Biotechnology, Austrian Academy of Sciences, Vienna, Austria

[6]Tissue Engineering Group, Department of Human Structure and Repair, Ghent University, Belgium

[7]Laboratory Experimental Cancer Research (LECR), Ghent University, Ghent, Belgium

[8]Institute of Biomedical Engineering, Department of Engineering Science, University of Oxford, Oxford, UK

[9]Applied Microfluidics for BioEngineering Research, MESA+ Institute for Nanotechnology and Technical Medical (TechMed) Center, University of Twente, Enschede, The Netherlands

*Equal contribution of last authors

Abstract

Ultrasound-triggered drug-loaded microbubbles have great potential for drug delivery due to their ability to locally release drugs and simultaneously enhance their delivery into the target tissue. We have recently shown that upon applying ultrasound, nanoparticle-loaded microbubbles can deposit nanoparticles onto cells grown in 2D monolayers, through a process that we termed “sonoprinting”. However, the rigid surfaces on which cell monolayers are typically growing might be a source of acoustic reflections and aspherical microbubble oscillations, which can influence microbubble-cell interactions. In the present study, we aim to reveal whether sonoprinting can also occur in more complex and physiologically relevant tissues, by using free-floating 3D tumor spheroids as a tissue model. We show that both monospheroids (consisting of tumor cells alone) and cospheroids (consisting of tumor cells and fibroblasts, which produce an extracellular matrix) can be sonoprinted. Using doxorubicin-liposome-loaded microbubbles, we show that sonoprinting allows to deposit large amounts of doxorubicin-containing liposomes to the outer cell layers of the spheroids, followed by doxorubicin release into the deeper layers of the spheroids, resulting in a significant reduction in cell viability. Sonoprinting may become an attractive approach to deposit drug patches at the surface of tissues, thereby promoting the delivery of drugs into target tissues.

Keywords

Microbubbles; Ultrasound; Drug Delivery; Loaded Microbubbles, Mechanisms; Sonoprinting

Graphical Abstract

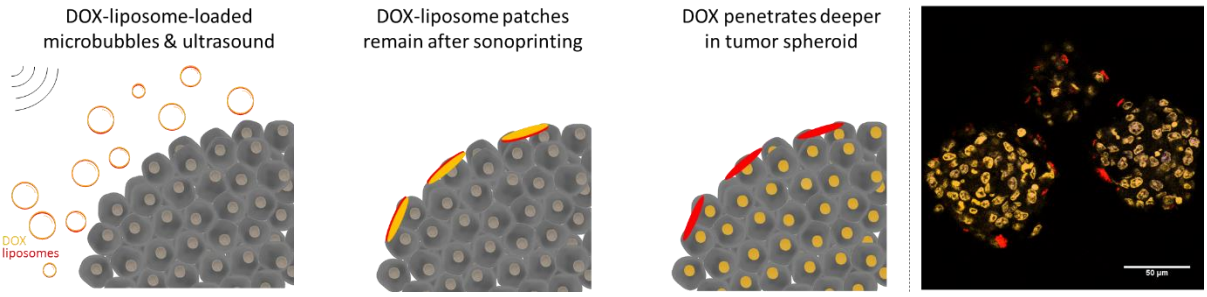

Introduction

Despite the wide range of anti-cancer agents available, successful clinical treatment of tumors remains challenging. One of the major reasons is the severe toxicity that can occur in healthy tissues due to the non-selective nature of anti-cancer drugs. An attractive solution is to encapsulate these drugs into nanometer-sized particles to localize their therapeutic effect. Nanomedicines are believed to preferably extravasate in tumorous tissue based on the enhanced permeation and retention (EPR) effect[1,2]. This selective uptake originates from enlarged openings in the poorly-organized endothelial barriers of fast growing tumors, and inefficient removal of products due to underdeveloped lymph vessels. However, the EPR effect has proven to be tumor type- and patient-dependent and can even be highly variable within a tumor[2–5]. Furthermore, tumor-associated fibroblasts can produce a very dense extracellular matrix, limiting the penetration of nanoparticles in the deeper layers of the tumor[2,6–8]. These factors are often ill-represented in preclinical tumor models, which could explain why so far only limited therapeutic benefits of nanomedicines are found in clinical studies[5,9,10]. Nanomedicines remain, however, very attractive due to their tunable nature; their ability to (i) improve the solubility and plasma half-life of (poorly soluble) drugs and (ii) protect bioactive substances, such as proteins and genetic drugs, from premature degradation while promoting their cellular uptake via endosomal pathways. To improve the intratumoral uptake of nanomedicines, active targeting approaches are currently under investigation[11–13]. Using physical triggers to achieve active nanoparticle delivery is of particular interest since it does not require the presence of specific ligands and it is not affected by changes in target expression. Possible physical stimuli that could induce local drug delivery include magnetism, thermal activity, light and ultrasound[2,13,14].

Here, we focus on ultrasound-triggered drug delivery since ultrasound is a well-known, cost-effective and relatively safe method amenable to both imaging and therapy. In contrast-enhanced ultrasound imaging the blood pool is infused with lipid-shelled micron-sized gas bubbles, named microbubbles, which respond to ultrasound by cavitating, i.e. expanding and contracting along with the pressure phases of the ultrasound wave[15–17]. The strong echo arising from cavitation makes microbubbles excellent contrast agents for imaging. Additionally, microbubbles are under investigation as drug

carriers, since ultrasound-induced cavitation can facilitate spatial and temporal control of drug release and has shown to promote the uptake of drugs and nanoparticles in cells and tissues[15]. Until recently, two main mechanisms were commonly believed to be responsible for this improved delivery: firstly, sonoporation, i.e. the formation of small pores in cell membranes and opening of tight junctions and, secondly, enhanced endocytosis[15,18,19]. We and others however showed that loading nanoparticles onto the microbubble shell can significantly improve their cellular uptake when compared to simply mixing these nanoparticles with microbubbles[20–24]. Since neither sonoporation, nor enhanced endocytosis could explain this, it was suggested that an alternative mechanism might be at play. In an earlier study[25], we introduced 'sonoprinting' as a mechanism to explain this observation. We found that nanoparticle-loaded microbubbles release their payload along with parts of the microbubble shell during cavitation, after which the translating microbubble gas core drags the nanoparticles in its wake and finally deposits them onto the cell membrane, hence the term sonoprinting (figure 1). Only recently, we elucidated the biophysical microbubble-cell interactions that are responsible for sonoprinting and identified the optimal acoustic settings to induce it[26]. This study was however performed on adherent cells cultured on a stiff membrane in a static *in vitro* setup, which can impact the observed microbubble behavior. Indeed, it has been shown that the presence of a solid boundary can cause aspherical microbubble oscillations, which may influence their interaction with the cells[27–29]. Furthermore, since sonoprinting was only studied on a single cell layer, questions on the significance of sonoprinting in a more physiologically relevant model remained. For these reasons, we investigate in the current study whether sonoprinting can also stimulate drug delivery in 3D tumor spheroids.

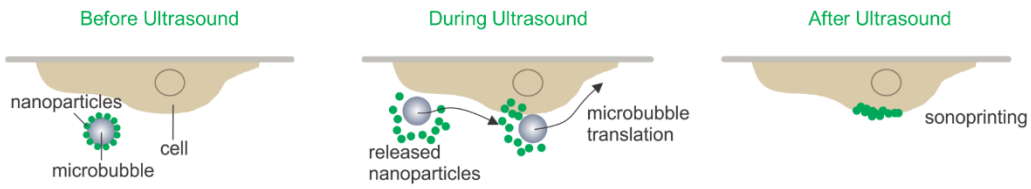

Figure 1: **The mechanism of sonoprinting**. Reproduced from Roovers et al. Biomaterials, 2019, with permission from Elsevier.

Compared to 2D cell monolayers, spheroids mimic the *in vivo* conditions more closely due to the enhanced cell-to-cell contact, while maintaining the controlled environment of an *in vitro* study[30–32]. Additionally, they can resemble the clinical situation even more by including multiple cell types that are typically found in the tumor microenvironment, such as tumor-associated fibroblasts and immune cells[5,8,32–34]. The 3D micro-environment in such cultures resembles clinical avascular tumor nodules, as an extracellular matrix is formed that may act as a major physical barrier for drug penetration[31]. Indeed, research has revealed that several treatments are less effective in 3D multicellular spheroids

than in 2D monolayer cultures, due to limitations in drug diffusion and due to the variable proliferative state of the cells in a 3D environment[30,31,35,36].

The aim of the current study is to investigate whether nanoparticle-loaded microbubbles and ultrasound can promote the delivery and cytotoxicity of drug-loaded nanoparticles into tumor spheroids. As such, we aim to verify whether sonoprinting can also occur in a complex tissue. We made use of 3D spheroids consisting of either tumor cells alone (monospheroids) or tumor cells cocultured with fibroblasts (cospheroids) to mimic the effect of tumor stroma. First, fluorescent polystyrene beads and 'empty' fluorescently labeled liposomes were coupled onto microbubbles and exposed to ultrasound to investigate if sonoprinting of beads/liposomes on 3D spheroids could be achieved. Afterwards, we prepared microbubbles loaded with doxorubicin-loaded liposomes (resembling either Doxil® or ThermoDOX®) to study drug release from the sonoprinted liposomes and the associated cytotoxic effects on the spheroids.

Materials and methods

Cell culture

4T1 murine breast cancer cells (ATCC, Manassas, VA, USA), 4T1 Luciferase positive cells (courtesy of the lab of Prof. Olivier De Wever) and NIH/3T3 fibroblast cells (ATCC) were grown in culture flasks in a humidified atmosphere with 5% CO_2 at 37°C. The culture medium for the 4T1 cells was RPMI (Gibco™, Thermo Fisher Scientific, Waltham, WA, USA), supplemented with 10% (v/v) fetal bovine serum (Hyclone, Thermo Fisher Scientific, MA, USA), 20 U/mL penicillin-streptomycin (Gibco™) and 2 mM L-glutamine (Gibco™). For the NIH/3T3 cells, Dulbecco's Modified Eagle Medium (Gibco™), with the same supplements was used.

Spheroid culturing and characterization

Multicellular tumor spheroids were made by harvesting NIH/3T3 and 4T1 cells using 0.25% (w/v) Trypsin - EDTA solution (Gibco™) and transferring them to a custom-made, agarose-based 400 µm microwell array, developed by the Rivron Lab (MERLN institute, Maastricht, The Netherlands)[37,38]. One microwell array chip was able to form 1500 spheroids, containing approximately 500 cells per spheroid. The microwells were either filled with 4T1 cells only (monospheroids) or NIH/3T3 and 4T1 cells in a 5:1 ratio (cospheroids), in accordance with previous work[7]. The cells were allowed to self-aggregate for 48h to form spheroids. After 48h, medium was removed and the spheroids were flushed out using fresh medium before being transferred to acoustically-transparent Lumox dishes (Sarstedt AG & Co. KG, Nümbrecht, Germany) that were sealed with water-impermeable acoustically transparent Sonolids, developed by the BUBBL group (Institute of Biomedical Engineering, Oxford University, UK)[39]. One dish was filled with approximately 1500 spheroids, suspended in 5 mL full medium. The cellular

organization of the NIH/3T3 and 4T1 cospheroids was examined by labeling NIH/3T3 cells with CellTrace™ Blue (excitation/ emission maxima: 355⁄410 nm, Molecular Probes™, Thermo Fisher Scientific, Waltham, WA, USA) and 4T1 cells with CellTrace™ Yellow (excitation/ emission maxima 546⁄579 nm, Molecular Probes™) prior to spheroid formation.

Microbubbles

Biotinylated microbubbles were composed of DPPC (1,2-dipalmitoyl-sn-glycero-3-phosphocholine) (Avanti Polar Lipids, Alabaster, AL, USA) and DSPE-PEG_{3400}-biotin (1,2-distearoyl-sn-glycero-3-phosphoethanol-amine-N-(biotinyl(polyethyleneglycol)-3400)) (Laysan Bio Inc, Arab, AL, USA) in a molar ratio of 85:15. Microbubbles without biotin were prepared as control samples (coadministration of microbubbles and liposomes) and were composed of DPPC and DSPE-PEG_{2000} (1,2-distearoyl-sn-glycero-3-phosphoethanol-amine-N-[(polyethyleneglycol)2000) (Laysan Bio Inc, Arab, AL, USA) in the same molar ratio. The microbubbles were prepared as described before[18,25,40]. In short, appropriate amounts of the lipids were dissolved in chloroform and transferred to a round bottom flask. After evaporation of the chloroform using a rotavapor at 65°C, the resulting lipid film was rehydrated in a preheated mixture of HEPES buffer (20 mM, pH 7.4), propylene glycol, and glycerol (ratio 7:2:1) to yield a final lipid concentration of 0.75 mg/mL. Aliquots of this lipid solution were transferred into 2.5 mL chromatography vials, of which the headspace was filled with inert C_4F_{10} gas (F2 chemicals, Preston, UK). Finally, microbubbles were obtained by high speed shaking of the lipid solution for 15s in a Capmix™ device (3 M-ESPE, Diegem, Belgium). The microbubbles were subsequently washed by centrifugation (750 g for 5 min at room temperature) using HEPES buffer. Afterwards, avidin (100 mg/mL, IBA GmbH, Göttingen, Germany) was added in excess and left to incubate for 5 min to couple to the biotin groups. The excess of avidin was removed by 2 cycles of centrifugation and finally the microbubbles were resuspended in HEPES buffer at a concentration of 10^9 microbubbles/mL, as determined by a Coulter Counter (Multisizer 4, Beckman Coulter Life Sciences, Indianapolis, IN, USA).

Biotinylated polystyrene beads

To evaluate the delivery of inert nanoparticles, yellow-green fluorescent carboxylate-modified polystyrene beads of 100 nm in size (excitation/emission: 505/515 nm, Molecular Probes™, Waltham, WA, USA) were coupled to the microbubble surface. To attach the beads to the biotinylated microbubble surface, the beads were covalently coated with polyethylene glycol-biotin via amine-coupling as described before[25]. To this end, 2 kDa biotin-PEG-amine (Creative PEGWorks, Winston Salem, NC, USA), N-(3-dimethylaminopropyl)-N'-ethylcarbodiimide hydrochloride (EDC) (Sigma Aldrich, Saint Louis, MO, USA), and N-hydroxysulfosuccinimide sodium salt (sulfo-NHS) (Sigma-Aldrich) were dissolved in HEPES Buffered Saline (HBS) (10 mM HEPES (Sigma-Aldrich), 150 mM NaCl (Sigma-Aldrich) containing 3.4 mM EDTA (Merck, Overijse, Belgium), 0.005% Tween 20 (Sigma-Aldrich) and

adjusted to pH 8). The fluorescent beads were added to this mixture to give final concentrations of 4 mg/mL EDC, 1.13 mg/mL Sulfo-NHS, 10 mg/mL biotin-PEG-amine and 1% w/V beads. The mixture was rotated overnight at room temperature. The PEG-biotin modified beads were purified by ultracentrifugation (Beckman Coulter Life Sciences) at 234000 g for 45 min and resuspended in HBS buffer to yield a concentration of 2% w/V beads. Afterwards, the zeta potential was measured by the Zetasizer Nano SZ (Malvern Panalytical) where an increase in the zeta potential of the negatively charged beads indicated partial shielding of the charge by the polymer coating and successful PEG-biotin coating.

Biotinylated liposomes

Regular liposomes were based on Doxil® and consisted of DPPC, DSPE-PEG_{3400}-biotin and cholesterol (Avanti Polar Lipids) in a molar ratio of 55:5:40, as previously reported by Lentacker et al.[24]. Thermosensitive liposomes were based on ThermoDOX® and consisted of DPPC, DSPE-PEG_{3400}-biotin and MSPC (1-myristoyl-2-stearoyl-sn-glycero-3-phosphocholine) (Avanti Polar Lipids) in a molar ratio of 85:5:10, as previously reported by Van Elk et al.[41]. 1 mol% of DiD (excitation/emission: 648/670 nm; Molecular Probes™, Thermo Fisher Scientific, Waltham, WA, USA) was added to the lipid mixture to fluorescently label the liposomes. Liposomes were prepared by transferring appropriate amounts of lipids dissolved in chloroform to a round bottom flask. Chloroform was removed via evaporation and HEPES buffer (20 mM, pH 7.4) was added to rehydrate the lipid film, resulting in a lipid concentration of 16 mg/mL. To reduce the liposome size, the lipid solution was sonicated in a bath sonicator (Branson Ultrasonics, Emerson, St. Louis, MO, USA) for 5 min. The final liposome size was determined on a Zetasizer Nano SZ (Malvern Panalytical, Worcestershire, UK).

Doxorubicin-loaded liposomes (DOX-liposomes) were prepared in the same way, but were resuspended in $(NH_4)_2SO_4$ buffer (250 mM, pH 5.5) for active loading of doxorubicin into the liposomes[42]. Afterwards, the external $(NH_4)_2SO_4$ buffer was removed via ultracentrifugation (L8-70M ultracentrifuge equipped with a SW55Ti Rotor, Beckman Coulter Life Sciences) at 35 000 rpm for 1h at 25°C for the regular DOX-liposomes; and via PD-10 columns (Sephadex G-25, GE Healthcare Life Sciences, Pittsburgh, PA, USA) in case of thermosensitive DOX-liposomes. Subsequently, a doxorubicin solution (10 mg/mL) was added to the liposomes in a 1:10 volume ratio and left to incorporate in the liposomes for 2h at 70°C in case of the regular liposomes and at 37°C in case of the thermosensitive liposomes. To remove the excess of free doxorubicin, a second ultracentrifugation step (35 000 rpm, 1h, 25°C) was performed and the DOX-liposomes were finally resuspended in HEPES buffer. The doxorubicin concentration in the liposomal dispersions was measured on an EnVision spectrophotometer (absorbance at 450 nm, Perkin-Elmer, Zaventem, Belgium). Therefore the liposomes were incubated with 10% Triton X-100 to release the doxorubicin from the DOX-liposomes

and the signal was compared to a calibration curve of doxorubicin solutions with known concentrations, in the presence of 10% Triton X-100. Furthermore, the concentration of liposomes (i.e. number of liposomes per mL) was determined using a NanoSight LM10 system (Malvern Panalytical). Knowing the doxorubicin concentration and the number of liposomes per mL of the liposomal dispersions, we were able to estimate the amount of doxorubicin per liposome.

Loading microbubbles with polystyrene beads/liposomes

To load the polystyrene beads/liposomes on the surface of the microbubbles, 50 µL of the biotinylated polystyrene beads or liposomes was added to 1 mL of the avidinylated microbubbles and allowed to incubate for 5 min. For the liposome-loaded microbubbles, the coupling efficiency was determined by measuring the concentration of free liposomes remaining in the liposome-microbubble dispersion, using the NanoSight LM10.

Ultrasound treatment of tumor spheroids

Ultrasound exposure experiments were performed in a water bath (37 °C) containing a rubber bottom layer to prevent reflections of the ultrasound beam (figure 2A). 100 µL of bead-loaded or liposome-loaded microbubbles was added to the Lumox plates containing approximately 1500 spheroids in suspension. The Lumox plates were radiated for 10s using a Sonitron device (Sonitron 2000; Rich-Mar, Inola, OK, USA) with a 1 MHz center frequency, at 2 W/cm² (corresponding to 700 kPa peak negative pressure), 10% duty cycle and 2000 cycles per pulse (figure 2B). In our previous work on 2D monolayers of cells, we found that these are optimal acoustic settings to achieve sonoprinting[25,26]. Following the ultrasound treatment, the Lumox plates were left to incubate in the cell incubator for 4h before analysis. A number of control samples were included as well. First, a “coadministration” sample, in which a physical mixture of 5 µL polystyrene beads or liposomes and 100 µL non-biotinylated microbubbles was transferred to the Lumox plates, followed by ultrasound treatment as described above. A second control contained 5 µL polystyrene beads (“bead only”) or liposomes (“liposome only”) and was not exposed to ultrasound. In the experiments where doxorubicin was encapsulated in the liposomes, a third “doxorubicin only” control was included, in which free doxorubicin was added to the Lumox plate in the same concentration as in the other samples containing doxorubicin, without ultrasound exposure. Note that in all the experiments with doxorubicin-containing samples an extra centrifugation step (5 min at 1100 rpm) was performed 15 min after ultrasound exposure, to remove any excess of free doxorubicin or doxorubicin-liposomes after treatment. After this centrifugation step all samples were heated for 15 min at 42°C, and subsequently left to incubate for 24h before analysis. In all microscopy experiments, Hoechst 33342 (Thermo Fisher Scientific, Waltham, WA, USA) was added 30 min before analysis in a 1:1000 ratio to visualize the cell nuclei.

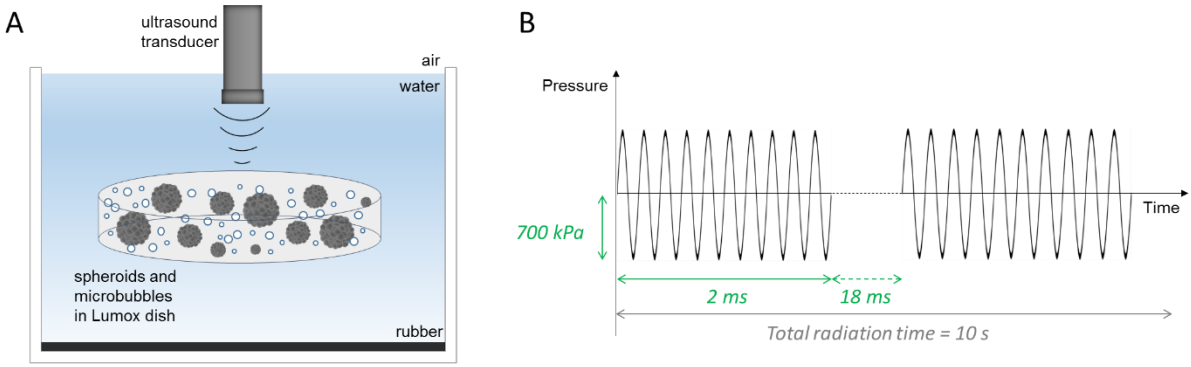

Figure 2: **Ultrasound treatment of spheroids. (A)** Schematic representation of the experimental set-up. Spheroids and microbubbles/liposomes were brought into ultrasound-transparent Lumox dishes, which were submerged in a water bath containing a rubber bottom layer and subsequently exposed to ultrasound radiations. **(B)** Schematic representation of the ultrasound treatment. 1 MHz ultrasound was applied for 10 s, at 2W/cm², corresponding to approx. 700 kPa, with 10% duty cycle and 2000 cycles (i.e. 2 ms) per pulse.

Flow cytometry

To analyze the delivery of liposomes to the spheroids, spheroids were first dissociated into a single cell suspension. Therefore, the spheroids were incubated with 1 mL of Trypsin - EDTA (0.25%, Gibco™) for 5 min, whereafter they were further disintegrated into single cells mechanically using a 21G needle (BD, Franklin Lakes, NJ, USA) attached to a 1 mL syringe (BD). Afterwards, the trypsin was neutralized by fresh culture medium and the single cell suspensions were finally resuspended in flow buffer (i.e. PBS-/- (Gibco™) supplemented with 1% of BSA (Sigma Aldrich) and 0.5% of NaN_3 (Sigma Aldrich). Flow cytometry data were acquired using a CytoFLEX (Beckman Coulter Life Sciences, Indianapolis, IN, USA) and analyzed using FlowJo™ software. During analysis, compensation for spectral overlap was performed and single cells were gated to remove the signals from remaining cell doublets and triplets.

The loading capacity of microbubbles with fluorescently-labeled liposomes was evaluated with flow cytometry as well. To this end, the liposomes were added to the microbubbles in the specified ratios (10; 20; 50 µL liposomes to 1 mL of microbubbles) and left to incubate for 5 min before analysis by flow cytometry. As before, flow cytometry data of microbubbles were acquired using a CytoFLEX and analyzed using FlowJo™ software. Gating was performed to selectively measure the microbubble-bound liposomal fluorescence.

Confocal microscopy

All confocal microscopy images were recorded on a C1-si confocal microscope (Nikon, Amsterdam, The Netherlands) equipped with a 60× water immersion objective (NIR Apo, Nikon) and a 10x air objective (Plan Apo, Nikon). A 405 nm laser was used to visualize Hoechst 33342/DAPI associated with the cellular nuclei; a 488 nm laser was used to excite fluorescent doxorubicin, while the emitted signal was

detected over the TRITC emission window. Finally, a 637 nm laser was used to visualize DiD, present in the liposomal bilayer. Confocal imaging was performed on 10 µm thick cryosections, as well as on intact spheroids. Living spheroids were transferred to glass-bottom microscopy grade dishes (CELLview™ cell culture dishes, Greiner Bio-One, Kremsmünster, Austria) for imaging. Optical cross-sections of the spheroids were acquired using the 60x objective with a 1 µm increment to produce Z-stacks of the entire spheroid volume. To determine the radial fluorescence plot profile in a single cross-section, the 'Radial Profile' plug-in for the image analysis software ImageJ (NIH, MD, USA) was used.

Histology

Paraffin-embedded sections

The spheroids were fixated in 4% paraformaldehyde (PFA) (VWR, Radnor, PA, USA), dehydrated through an ethanol concentration gradient and embedded in paraffin. Sections of 5 µm thickness were cut (Cut4060; Slee Medical, Mainz, Germany) and deparaffinized. Histological staining was done using a standard protocol for hematoxylin-eosin to evaluate cell morphology. The presence of extracellular matrix in the spheroids was tested by collagen I staining (1:150, R1086, Acris Antibodies GmbH, Herford, Germany). In short, the sections were enzymatically digested by incubation with 1 mg/mL pepsin at 37°C for 30 min, followed by 2h of incubation with a monoclonal mouse anti-collagen I antibody after pretreatment with 3% H_2O_2 for 10 min and blocking with BSA and 4% normal rabbit serum in PBS. Afterwards streptavidin-peroxidase was added for 30 min before a secondary antibody (biotinylated swine anti rabbit, 1:200, E2431, Dako, Agilent Technologies, Santa Clara, CA, USA) was introduced. Finally, the sections were incubated with DAB for 10 min and counterstained with hematoxylin. Imaging was subsequently performed on an Olympus BX51 microscope.

Cryosections

Spheroids were fixated in 4% PFA for 30 min prior to embedding in Tissue-Tek® O.C.T. (Sakura Finetek USA Inc, Torrance, CA, USA). The spheroids were subsequently snap-frozen with liquid nitrogen and 10 µm sections were prepared using a Cryotome® FSE (Thermo Fisher Scientific, Cheshire, UK) and allowed to adhere to Superfrost microscopic glass slides (Menzel-Gläser, Braunschweig, Germany). The sections were air dried for 20 min before adding DAPI-containing mounting medium. The cryosections were visualized under confocal microscopy as described before.

Cell viability assays

To estimate the spheroid viability after treatment, an ATP-based CellTiter-Glo® 3D Cell Viability Assay (Promega Corporation, Madison, WI, USA) that is optimally adapted for the evaluation of toxicity in 3D cell cultures[43], was performed. For this, the spheroids were transferred to low adherent gyratory shaker flasks after treatment and placed on a shaker plate at 37°C and 70 rpm, to remain in 3D culture until analysis. After 72h, the spheroids were incubated with the CellTiter-Glo® 3D reagent and analyzed

as described by the manufacturer, using a GloMax® 96 Microplate luminometer (Promega). Cell viability was normalized against untreated spheroids.

To selectively evaluate the viability of tumor cells within the mono- and cocultures, a firefly luciferase assay was performed on spheroids containing Luciferase positive 4T1 cells. As for the CellTiter-Glo® assay, the spheroids were kept in 3D cultures after treatment by gyratory shaking for 72h. Afterwards, the spheroids were incubated with a 5x dilution of Luciferase Cell Culture Lysis 5X Reagent (Promega) for 20 min. The resulting solution was transferred to a white flat-bottom 96-well plate (Corning Incorporated, Corning, NY, USA) and the 4T1-derived luciferase activity was determined using the Luciferase Assay System from Promega. A CLARIOstar luminometer (BMG Labtech, Cary, NC, USA) with injection system was programmed to perform a 2s delay, follow by a 10s read-out, as instructed by the manufacturer.

Incucyte® live cell analysis

Spheroid morphology was evaluated using the IncuCyte® ZOOM System ((Essen Bioscience, Hertfordshire, UK) over 72h. For this, a single spheroid was handpicked under a light microscope (Wild Heerbrugg, Heerbrugg, Switzerland) and transferred to a Corning® 96-well Clear Round Bottom Ultra-Low Attachment Microplate (Corning Incorporated, Corning, NY, USA) containing 100 µL full medium. The plate was inserted in the Incucyte ZOOM System and images at 10x magnification were taken every 1,5 to 2h for 72h.

Statistical analysis

All experiments were performed independently on different days with a minimum of 3 biological replicates. Statistical analysis was performed using one-way ANOVA analysis with a Bonferroni's multiple comparison test, as calculated by GraphPad Prism 6 (GraphPad software, San Diego, CA, USA) and expressed as the mean ± standard deviation.

Results

Generation of mono- and cospheroids

Spheroids were generated using an 400 µm agarose-based microwell array platform, as developed by Vrij et al[37], in which single cells assemble into multicellular spheroid cultures of approximately 100 to 150 µm in size within 48h (figure 3A). Based on earlier work by Priwitaningrum et al.[7] we prepared 4T1 breast cancer monospheroids and cospheroids consisting of 4T1 breast cancer cells and NIH/3T3 fibroblasts in a 1:5 ratio. The addition of fibroblasts yields a more biologically relevant model due to the formation of extracellular matrix, which resembles the stroma found in various breast cancer phenotypes[7].

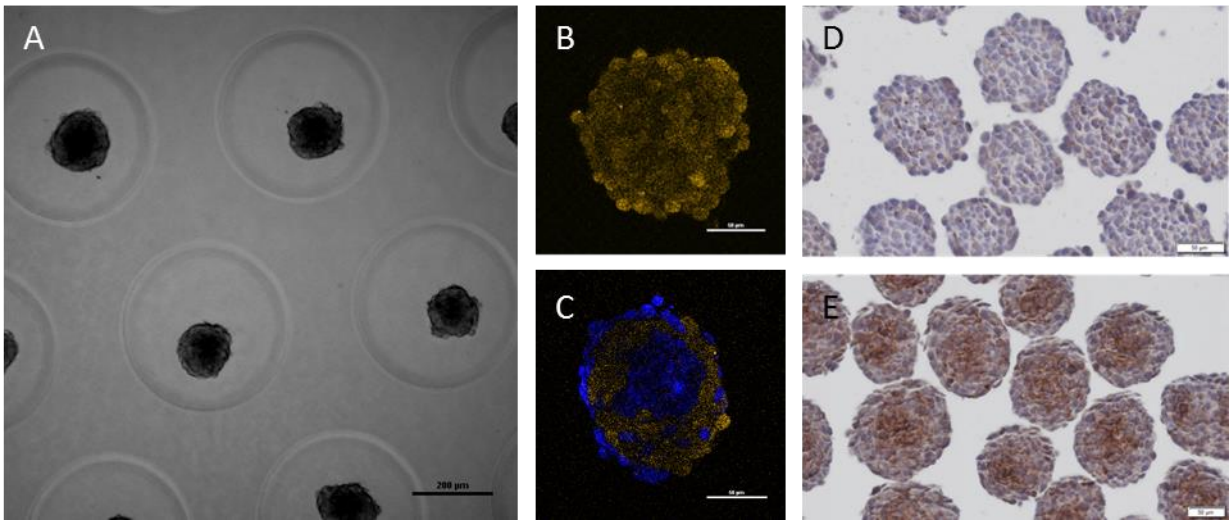

Figure 3: **Mono- and cospheroids. (A)** Bright-field image of cospheroids grown in microwells (grey circles) after 48h. The scale bar represents 200 µm. **(B&C)** Confocal images of **(B)** a monospheroid consisting of only 4T1 tumor cells, labeled with CellTrace™ Yellow, and **(C)** a cospheroid consisting of 4T1 tumor cells and NIH/3T3 fibroblasts in a 1:5 ratio, differentially labeled with CellTrace™ Yellow and CellTrace™ Blue, respectively, 48h after seeding (cross-section at 25-30 µm from the top). The scale bar represents 50 µm. **(D&E)** Collagen-1 staining (brown) on paraffin sections (cells in violet) of **(D)** monospheroids showing little to no collagen formation and **(E)** cospheroids indicating the presence of an extracellular matrix. The scale bar represents 50 µm.

To characterize the cellular organization of the spheroids, NIH/3T3 and 4T1 cells were labeled with two different CellTrace™ dyes prior to spheroid formation and the spheroids were subsequently imaged by confocal microscopy, as shown in figure 3B&C. Figure 3B and C show the localization of 4T1 cells (yellow) and NIH/3T3 cells (blue) in mono- and cospheroids respectively. Due to differences in cellular density and in intercellular adhesiveness, the fibroblasts tend to cluster among themselves and to accumulate within the center and on the outer part of the spheroids[36,44]. To confirm that the fibroblasts formed an extracellular matrix, we investigated the presence of collagen-1 in both mono- and cospheroids, as seen in figure 3D and 3E. While collagen-1 (brown color) is abundantly present in the cospheroids (figure 3E), almost no collagen-1 could be found in the monospheroids (figure 3D). Additionally, the collagen-1 is predominantly found in the center of the cospheroids which is in accordance with the confocal images showing that a high concentration of fibroblasts was found in this area.

Sonoprinting of model nanoparticles on tumor spheroids

In previous work, we showed that the ultrasound-triggered delivery of nanoparticles to cells growing in 2D monolayers was significantly enhanced when the nanoparticles were loaded onto the microbubble shell; we termed this phenomenon sonoprinting (figure 1)[25]. To determine if sonoprinting also occurs on free-floating 3D spheroids, and in the absence of ultrasound-reflecting membranes, we loaded two types of nanoparticles onto microbubbles using a biotin-avidin-biotin link. Figure 4 shows

confocal microscopy images of fluorescent polystyrene bead-loaded (figure 4A) and DiD-labeled liposome-loaded microbubbles (figure 4B) and their size distribution, as determined by Coulter Counter (figure 4C). The size of the microbubbles ranged from 1 to 10 µm, with an average size of 2.5 µm for unloaded microbubbles and 2.6 µm and 2.8 µm for liposome-loaded and bead-loaded microbubbles, respectively. The size and polydispersity index (pdI) of the different nanoparticles used in this study are summarized in supplementary table 1.

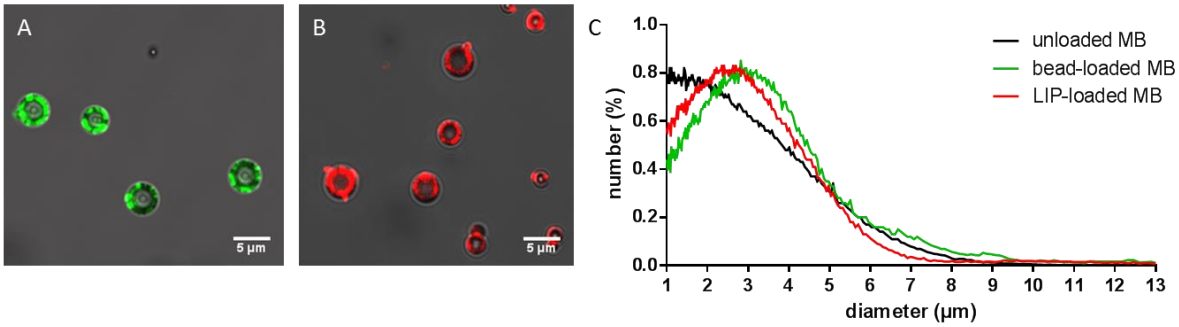

Figure 4. **Characterization of nanoparticle-loaded microbubbles. (A-B)** Confocal image of microbubbles loaded with **(A)** yellow-green fluorescent 100 nm polystyrene beads (green) and **(B)** DiD-labeled liposomes (LIP) (red). The scale bars represent 5 µm. **(C)** Size distribution of unloaded (black), polystyrene bead-loaded (green) and liposome-loaded (red) microbubbles, as determined via Coulter Counter.

First, biotinylated fluorescent polystyrene beads were used as model nanoparticles as they are inert and do not leak the entrapped dye. Flow cytometry analysis of the spheroid-derived cells 4h after treatment revealed that loading the beads on the microbubbles significantly improved their delivery to the spheroid-derived cells, when compared to the beads-only sample and the coadministration sample (figure 5B, black bars). These results collectively confirm that sonoprinting cannot only occur in 2D cell cultures but also on free-floating 3D tumor spheroids. An almost identical result was obtained in the case of cospheroids (figure 5C, black bars) which suggests that the tumor stroma has no impact on the sonoprinting process.

The same experiments were repeated with fluorescently (DiD) labeled liposomes, which are highly versatile drug carriers able to encapsulate both low molecular weights drugs (chemotherapeutics, corticosteroids) and complex biological therapeutic agents (mRNA, siRNA)[2,45–47]. As presented in figure 5B and C (grey bars), the delivery of liposomes to the cells of the mono- and cospheroids clearly improved upon binding the liposomes to the microbubbles, similar as observed for the polystyrene beads.

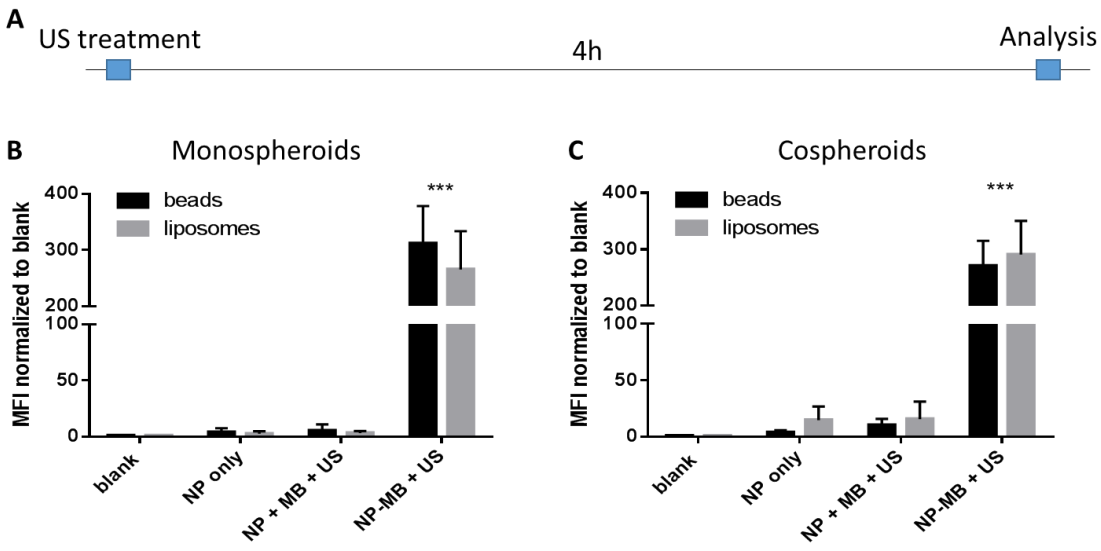

Figure 5: **Sonoprinting of polystyrene beads and liposomes on tumor spheroids. (A)** Time diagram: 4h after ultrasound treatment, the spheroids were analyzed by flow cytometry. **(B-C)** Normalized (to blank) mean intensity fluorescence (MFI; as determined by flow cytometry) of spheroid-derived cells from **(B)** monospheroids and **(C)** cospheroids. NP = nanoparticles; MB = microbubbles; US = ultrasound; NP + MB + US = nanoparticles and microbubbles coadministered and exposed to ultrasound radiation; NP-MB + US = nanoparticles loaded onto the microbubbles and exposed to ultrasound (i.e. sonoprinting). Significance levels are determined using a Bonferroni multiple comparison test: *** represents P<0.001.

However, since single cell suspensions are required for flow cytometric analysis, the results in figure 5 do not reveal where in the 3D spheroids the polystyrene beads or liposomes were delivered. Consequently, we further investigated the location of the fluorescent liposomes within the tumor monospheroids by confocal microscopy, as shown in figure 6. To this end, individual cross-sections (as illustrated in figure 6H) over the entire depth of the spheroid were made with a 1 µm increment, from which the entire spheroid could be reconstructed (as illustrated in figure 6G). In correspondence with the flow cytometry results (figure 5), the reconstructed volume views of the spheroids in figures 6B-E indicate that loading of the liposomes on the microbubbles and subsequent ultrasound treatment significantly enhanced the delivery of liposomes to the tumor spheroids (figure 6E). This is in sharp contrast to spheroids that were treated with liposomes alone (figure 6C) and coadministered liposomes and microbubbles (figure 6D). The individual cross-sections at increasing depth of the spheroid treated with liposome-loaded microbubbles and ultrasound are shown in figure 6F and revealed that liposome penetration is restricted to the outer layers of the tumor spheroid. As the tumor spheroids were on average 150 µm in size and light penetration is typically limited to a few tens of microns[36,48,49], it was impossible to visualize the inner part of the tumor spheroids by confocal microscopy. This is also clear from the radial fluorescence profile plot (figure 6I), derived from the cross-section at 40 µm in figure 6F. The plot illustrates that the nuclear staining (blue line, figure 6I)

could be retrieved in deeper layers of the tumor spheroid compared to the fluorescent liposome signal (red line), despite the fact that the 637 nm laser light used to excite the liposomes has a better tissue penetration than the 405 nm laser light used to excite the Hoechst nuclear stain[50]. These results confirm that the loss in liposomal signal at deeper locations in the spheroids is not due to a loss in fluorescence, though attributed to the fact that the liposomes are indeed printed superficially on the tumor spheroid. Together, these results indicate that liposomes can be sonoprinted on free-floating 3D tumor spheroids, yet the delivery remains restricted to the outer cell layers of the spheroids.

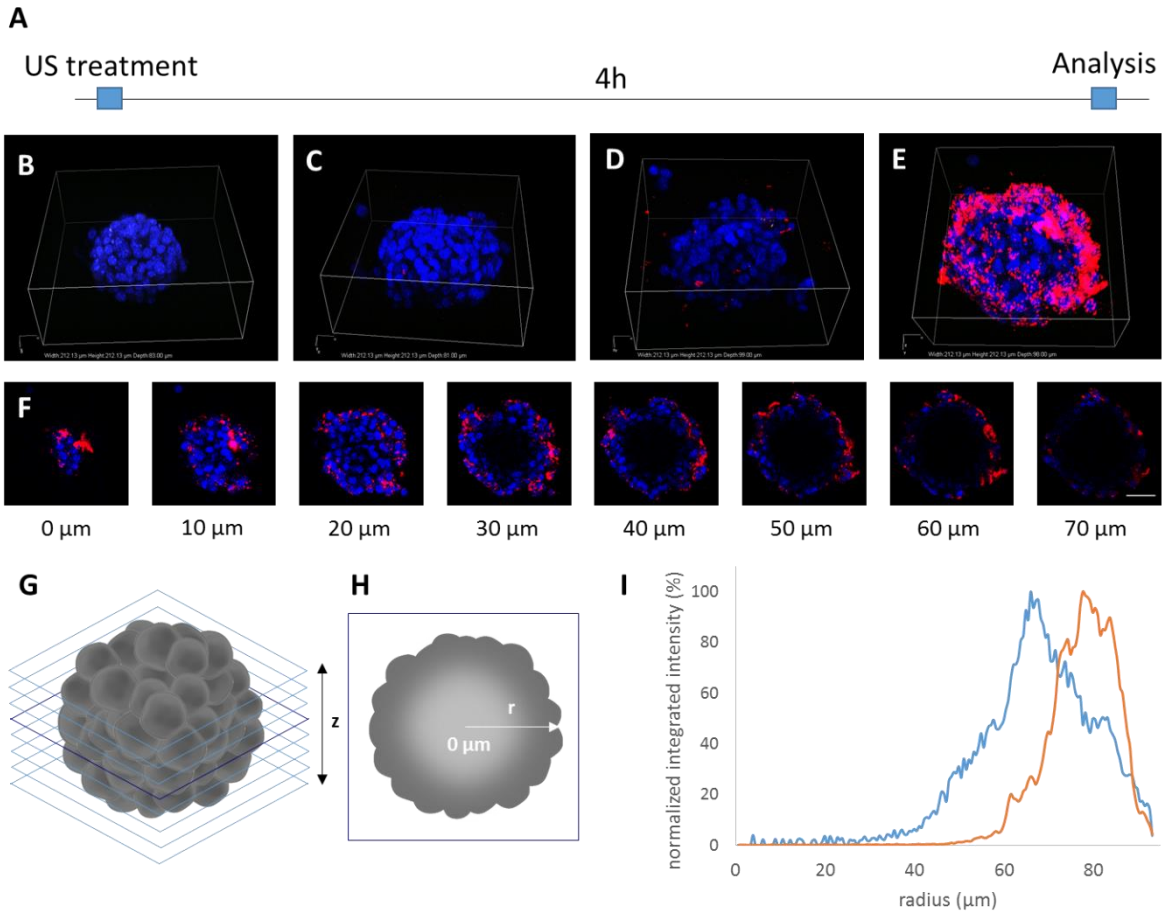

Figure 6: **Sonoprinting on 4T1 tumor monospheroids**. Blue = Hoechst 33342 nuclear stain, red = liposomes (DiD). **(A)** Time diagram: 4h after ultrasound treatment, the spheroids were analyzed by confocal microscopy. **(B-D)** Maximum intensity projections of confocal Z stacks taken from **(B)** an untreated spheroid, **(C)** a spheroid exposed to DiD-labeled liposomes only, **(D)** a spheroid exposed to DiD-labeled liposomes and microbubbles coadministered and exposed to ultrasound and **(E)** a spheroid exposed to DiD-labeled liposomes coupled onto microbubbles and exposed to ultrasound (i.e. sonoprinting). The dimensions of the white boxes are: 212 µm x 212 µm x 90 µm. **(F)** Individual cross sections of the spheroid in (E) at increasing depth. The center of the spheroid cannot be visualized by confocal microscopy due to limited light penetration. The scale bars represent 50 µm. **(G)** The maximum intensity projection of the spheroid is composed from stacks of cross sections in the z direction. **(H)** The radial profile plot is created by measuring the fluorescence profile over radius r over the entire spheroid. **(I)** Radial profile plot of the nuclear stain (blue) and the liposomal stain (red) from the spheroid center (0 µm) to the edges.

Doxorubicin release from sonoprinted DOX-liposomes

To investigate delivery of drugs subsequent to sonoprinting, we included the chemotherapeutic doxorubicin (DOX) in the liposomes. Doxorubicin is a small drug that can easily cross cell and nuclear membranes to reach the nucleus where it intercalates in DNA to exert its cytotoxic function. First, we estimated the amount of doxorubicin per liposome to be 3,1 x 10^{-10} µg doxorubicin/liposome on average, which is comparable to the doxorubicin content of clinically approved Doxil®[51]. The active loading of doxorubicin into the liposomes increased their size to approximately 200 nm (supplementary table 1). In these experiments, spheroids were treated with either free doxorubicin, DOX-liposomes only or DOX-liposomes either coadministered with or coupled onto microbubbles. In all samples, the doxorubicin concentration was kept identical. In case DOX-liposomes were coupled onto the microbubbles, we calculated that 1,6 x 10^{-7} µg doxorubicin was loaded onto each microbubble, based on the microbubble concentration (1,118 x 10^{9} per mL) and the concentration of unbound liposomes in the solution (4 x 10^{11} per mL, corresponding to approx. 45% of the total amount liposomes in the solution), as outlined in materials and methods.

As doxorubicin is a fluorescent molecule, both the drug-derived fluorescence and the liposome-derived fluorescence on the spheroid-derived cells could be individually measured by confocal imaging and flow cytometry (figure 7). The scatter plot presented in figure 7B, clearly indicates that more liposomes (y-axis) and doxorubicin (x-axis) were delivered to the monospheroid-derived cells 24h after treatment, only when exposed to DOX-liposome-loaded microbubbles and ultrasound (dark green dots). This population still exhibits a clear gradient in fluorescence, suggesting that the position of the cell within the spheroid strongly influenced to which extent liposomes/doxorubicin were taken up. This corresponds to the data in figure 6 where cells located in the outer layers of the spheroids showed a higher uptake of fluorescent liposomes. We also noticed a strong correlation between the liposomal and doxorubicin fluorescence, which suggests that intact DOX-liposomes were printed on the tumor spheroids and still contained the doxorubicin 24h after being printed. As expected, free doxorubicin (dark blue dots) penetrates the tumor spheroids very well, while the coadministration sample (light green dots) and liposome-only sample (orange dots) overlap and only show a modest increase in both liposomal and doxorubicin fluorescence. The corresponding histograms can be found in supplementary figure 1A,C,E,G and confirm that the treatment with DOX-liposome-loaded microbubbles and ultrasound resulted in an increased delivery of liposomal DiD and doxorubicin to the spheroid cells, even though differences in doxorubicin delivery are more difficult to distinguish due to the relatively low fluorescence of doxorubicin, which is moreover quenched by incorporation into liposomes[52]. While the overall shifts in MFI were less, a similar trend was found in cospheroids (figure 7C and supplementary figure 1E,G).

Doxil® liposomes are known to be highly stable towards drug leakage, for up to 2 weeks *in vitro*[42,51,53,54]. As the regular DOX-liposomes have a similar composition to Doxil®, it is difficult to experimentally verify whether doxorubicin can leak from the regular DOX-liposomal prints and penetrate into the deeper-lying tissue. Therefore, we prepared a thermosensitive DOX-liposomal formulation resembling ThermoDOX®, which is currently in phase III clinical trials[41]. These liposomes contain the lysolipid MSPC, which enables the disintegration of the liposomal structure upon heating to 42°C (*i.e.* the T_m of MSPC) and, consequently, the release of encapsulated doxorubicin. Tumor spheroids were treated with the same samples as in Figure 7B&C, though instead of regular DOX-liposomes, thermosensitive DOX-liposomes were used. Due to the heating (15 min at 42°C), doxorubicin was able to leak out of the thermosensitive DOX-liposomes. The scatter plots of monospheroids (figure 7F) and cospheroids (figure 7G) exposed to thermosensitive DOX-liposome-loaded microbubbles and ultrasound revealed that part of the doxorubicin was indeed able to leak out of the liposomal prints, as the correlation between liposomal and DOX fluorescence became less prominent (dark green dots). Moreover, as the doxorubicin fluorescence is no longer quenched, an enhancement in the fluorescence signal can be seen after doxorubicin was released from the thermosensitive liposomes. Furthermore, cells derived from tumor spheroids treated with free DOX-liposomes (orange dots) or the coadministration sample (light green dots) also showed a higher fluorescence intensity of doxorubicin and liposomal DiD (figure 7F&G and supplementary figure 1B,D,F,H). This could possibly be due to a release of the lipophilic DiD dye from liposomal fragments that remain after washing and a dequenched fluorescence of the released doxorubicin in these samples. Still, coupling thermosensitive DOX-liposomes onto microbubbles significantly improved the delivery. Again, a trend toward lower delivery in the cospheroids was seen when comparing the histograms of monospheroids to cospheroids (supplementary figure 1B,D,F,H).

To confirm these results and get a better view on the localization of the liposomes and the doxorubicin within the tumor spheroids, we made cryosections of the tumor spheroids 24h after ultrasound treatment, and imaged them with confocal microscopy (figure 7D,E,H,I and supplementary figure 2). The localization of liposomes (red fluorescence) and doxorubicin (orange fluorescence) within the spheroids was investigated after sonoprinting of both regular (figure 7D-E) and thermosensitive (figure 7H-I) DOX-liposomes. The individual fluorescence channels can be found in supplementary figure 3. For regular DOX-liposomes, the liposomal signal clearly overlaps with the doxorubicin fluorescence and both signals are limited to the outer layers of the spheroids (figure 7D-E), as was expected considering the slow doxorubicin release from such liposomes[42,51,53,54]. In contrast, the cryosections of spheroids sonoprinted with the thermosensitive formulation (figure 7H-I) confirmed that, following a short heating, doxorubicin was able to leak out of the liposomes and penetrate further into the tumor

spheroid. Contrarily to what has been reported before[55,56], the presence of the stroma in the cospheroids did not hamper the doxorubicin penetration in the cospheroids (figure 7I), indicating that, once release from the liposomes, doxorubicin is able to easily penetrate this stromal barrier. The cryosections from both mono- and cospheroids treated with DOX-liposomes only or DOX-liposomes coadministered with microbubbles and exposed to ultrasound, only showed limited doxorubicin fluorescence within the tumor spheroids (supplementary figure 2). Again, a minor increase in doxorubicin fluorescence in the spheroid cells treated with the thermosensitive DOX-liposome samples is visible, indicating that a small fraction of liposomes was still present in the samples after centrifugation.

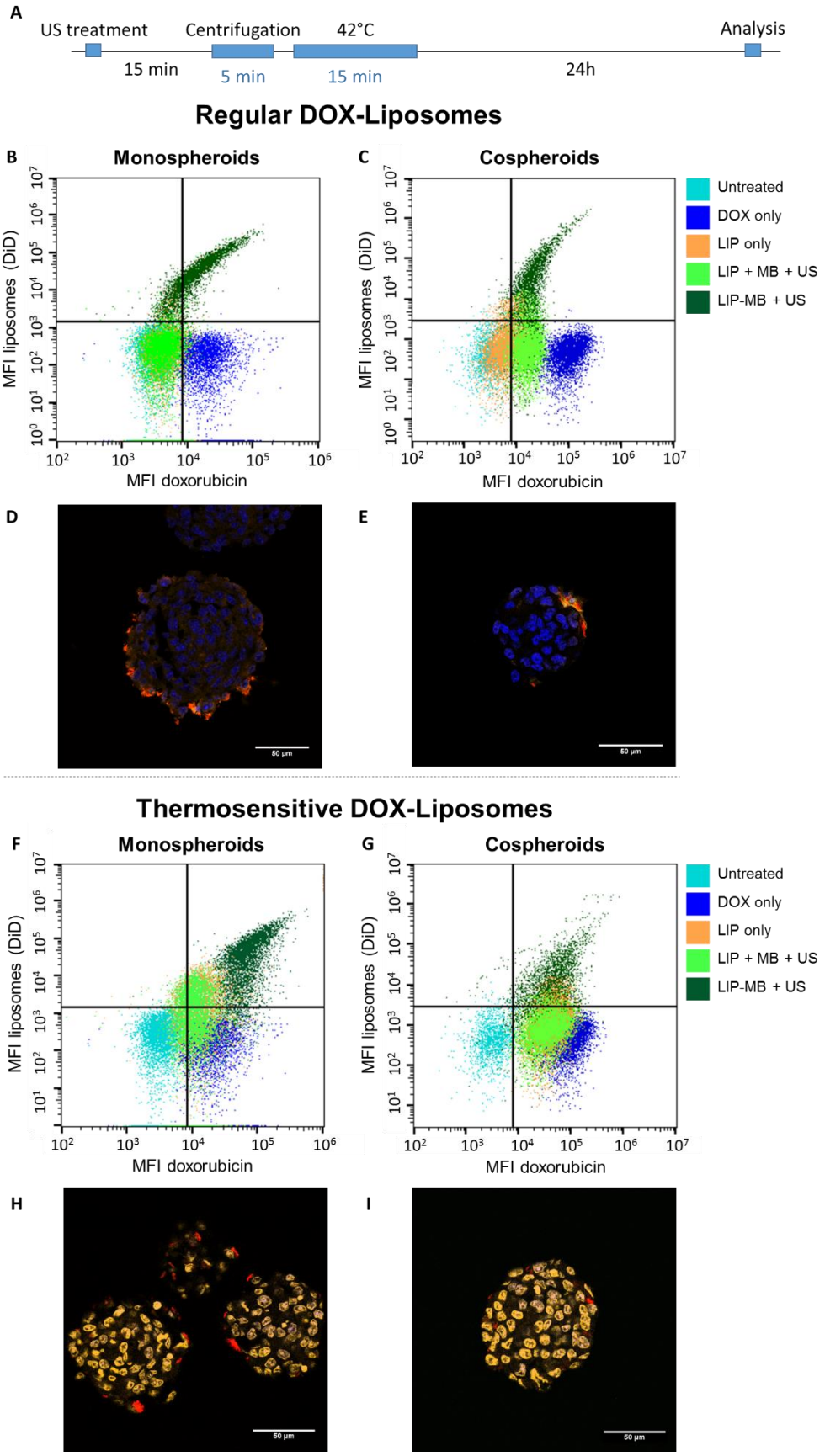

Figure 7: **Localization of doxorubicin after sonoprinting and a short heating step. (A)** Time diagram: 15 min after ultrasound treatment, the spheroids were centrifuged to remove any remaining free doxorubicin or DOX-liposomes. Subsequently, the

spheroids were exposed to 42°C for 15 min. After 24h, the spheroids were analyzed by flow cytometry and confocal microscopy on cryosections. **(B,C,F,G)** Flow intensity scatter plots of the cellular delivery of doxorubicin (doxorubicin fluorescence, horizontal axis) and **(B-C)** regular and **(F-G)** thermosensitive liposomes (DiD fluorescence, vertical axis) in **(B&F)** monospheroids and **(C&G)** cospheroids. DOX = doxorubicin; LIP = DOX-liposomes; MB = microbubbles; US = ultrasound; LIP + MB + US = DOX-liposomes and microbubbles coadministered before ultrasound radiation; LIP-MB + US = DOX-liposomes loaded onto the microbubbles and exposed to ultrasound (i.e. sonoprinting). **(D,E,H,I)** 10 µm cryosections of **(D&H)** monospheroids and **(E&I)** cospheroids treated with **(D-E)** regular or **(H-I)** thermosensitive DOX-liposomes coupled onto microbubbles and exposed to ultrasound. Blue = DAPI, orange = doxorubicin, red = liposomes (DiD). The scale bars indicate 50 µm.

Cytotoxicity of sonoprinted DOX-liposomes

To evaluate the cytotoxic effect of the printed DOX-liposomes, morphological changes in mono- and cospheroid were monitored during 72h after treatment with DOX-liposome-loaded microbubbles and ultrasound. Figure 8B&D show that untreated mono- and cospheroids grew similarly in size over time. In contrast, clear morphological differences between monospheroids and cospheroids treated with DOX-liposome-loaded microbubbles and ultrasound were seen (figure 8C&E): while monospheroids desintegrated (figure 8C), cospheroids mainly shed cell fragments (figure 8E). Highly likely, this can be explained by the presence of the extracellular matrix in the cospheroids that keeps the spheroid together.

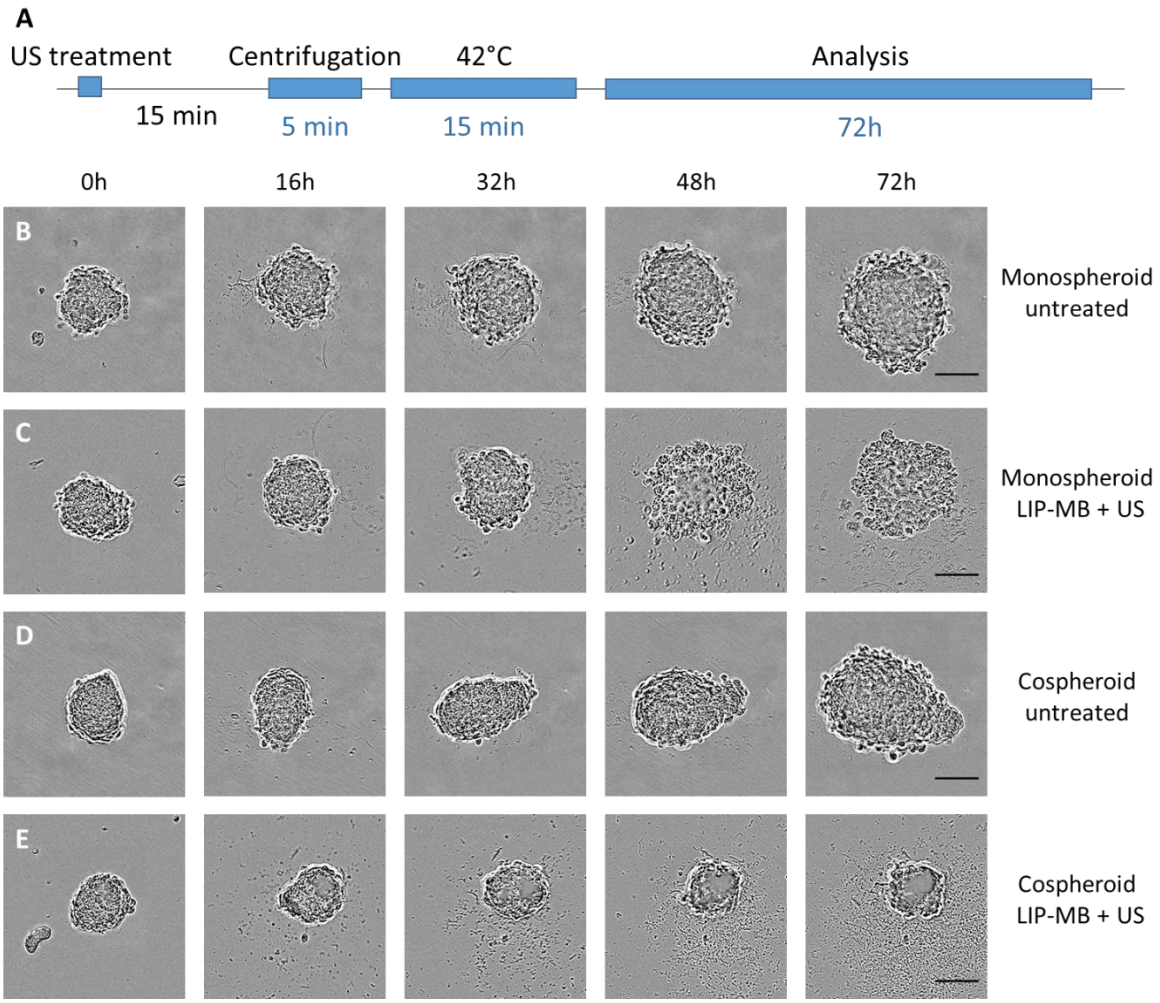

Figure 8: **Spheroids monitored over 72h after treatment. (A)** Time diagram: 15 min after ultrasound treatment, the spheroids were centrifuged to remove any remaining free doxorubicin or DOX-liposomes. Subsequently, the spheroids were exposed to 42°C for 15 min. Afterwards, the spheroid morphology was followed over a period of 72h. Phase contrast images of **(B)** untreated monospheroids and **(C)** monospheroids treated with regular DOX-liposomes coupled onto microbubbles and exposed to ultrasound (LIP-MB + US). **(D)** Untreated cospheroids and **(E)** cospheroids treated with regular liposomes coupled onto microbubbles and exposed to ultrasound (LIP-MB + US). The scale bars indicate 50 µm.

Based on these images, it is clear that it is more convenient to analyze cell toxicity at a later time-point, , as is expected from the fact that doxorubicin works by inhibiting DNA synthesis and will therefore only be effective on dividing cells. Therefore, we subsequently assessed the total cell viability of the tumor spheroids 72h after treatment, using a CellTiter-Glo® 3D Cell Viability Assay. Figure 9 shows the results obtained on monospheroids (figure 9B) and cospheroids (figure 9C).

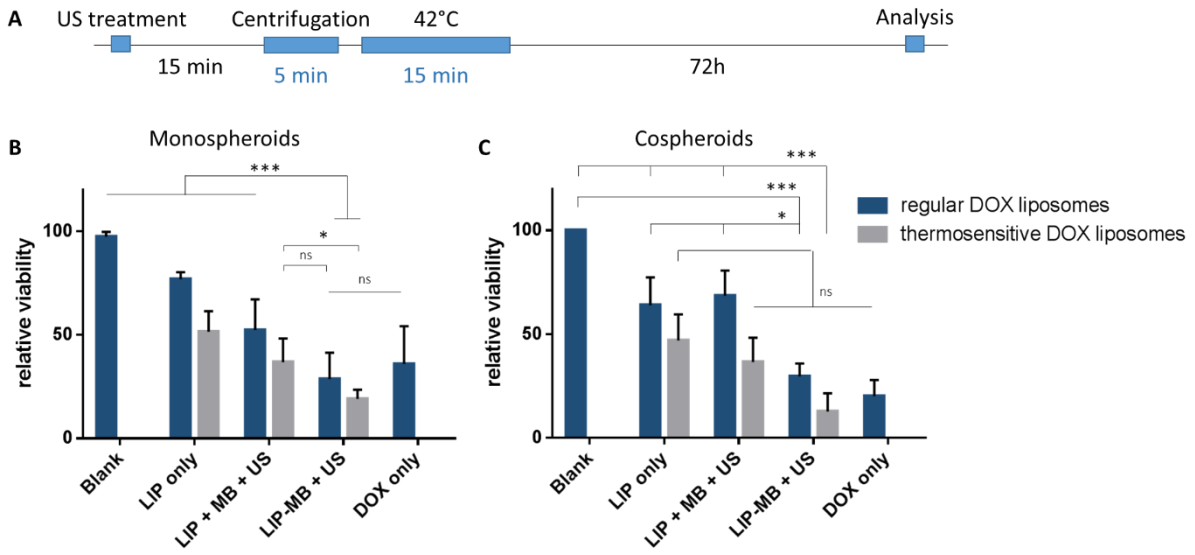

Figure 9: **Total cell viability of tumor spheroids 72h after treatment. (A)** Time diagram: 15 min after ultrasound treatment, the spheroids were centrifuged to remove any remaining free doxorubicin or DOX-liposomes. Subsequently, the spheroids were exposed to 42°C for 15 min. After 72h, the spheroids were analyzed using a CellTiter-Glo® 3D Viability Assay. **(B)** Cell viability after treatment of **(A)** monospheroids and **(B)** cospheroids. DOX = doxorubicin; LIP = DOX-liposomes; MB = microbubbles; US = ultrasound; LIP + MB + US = DOX-liposomes and microbubbles coadministered before ultrasound radiation; LIP-MB + US = DOX-liposomes loaded onto the microbubbles and exposed to ultrasound (i.e. sonoprinting). Significance levels are determined using a Bonferroni multiple comparison test: ns for $P>0.05$, * for $P<0.05$, ** for $P<0.01$, *** for $P<0.001$.

Sonoprinting of DOX-liposome-loaded microbubbles resulted in a significantly cytotoxicity compared to the liposomes alone and the liposomes coadministered with microbubbles and exposed to ultrasound, and was equally effective as free doxorubicin. Moreover, in contrast to the control samples where the thermosensitive DOX-liposomes (grey bars) appeared more toxic than the regular liposome samples (blue bars), this effect was observed for both regular and thermosensitive DOX-liposomes when coupled onto microbubbles and exposed to ultrasound. This suggests that doxorubicin must have been able to leak from the regular DOX-liposomes at a later time point as free doxorubicin was not yet detected in the cryosections 24h after treatment (figure 7). To confirm this, additional cryosections of monospheroids were made at different time points after treatment with DOX-liposome-loaded microbubbles and ultrasound and imaged by confocal microscopy (figure 10). Doxorubicin leakage from the thermosensitive liposomal patches occurred within 4h (figure 10B) while DOX release from the regular liposomes only started 48h after sonoprinting (figure 10C), confirming that DOX eventually leaked out of the regular liposomes as well.

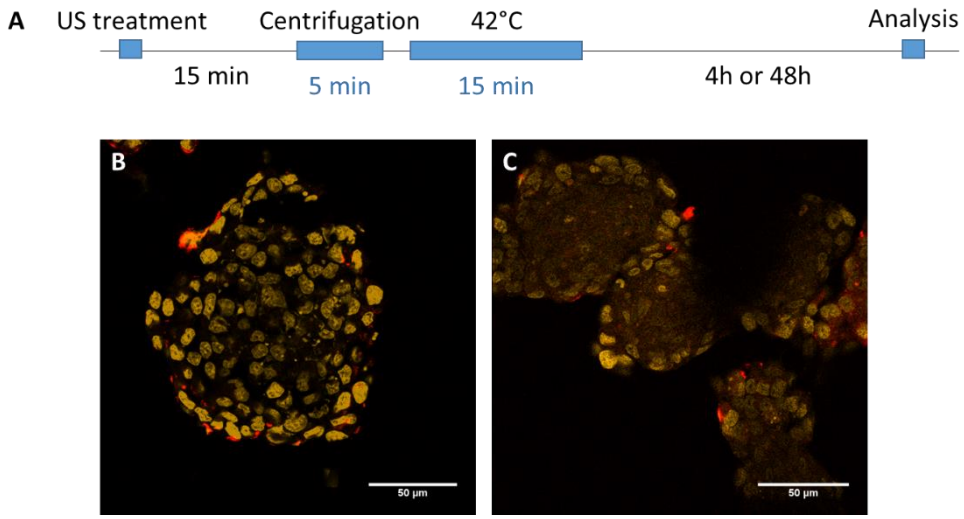

Figure 10: **Doxorubicin release from sonoprinted liposomal patches. (A)** Time diagram: 15 min after ultrasound treatment, the spheroids were centrifuged to remove any remaining free doxorubicin or DOX-liposomes. Subsequently, the spheroids were exposed to 42°C for 15 min. After **(B)** 4h for thermosensitive DOX-liposomes or **(C)** 48h for regular DOX-liposomes, the spheroids were analyzed by confocal microscopy on cryosections. Orange = doxorubicin, red = liposomes (DiD). The scale bars indicate 50 µm.

The presence of fibroblasts in cancerous tissues can have a pro-carcinogenic effect, partly due to the formation of a dense extracellular matrix that acts as a physical transport barrier for drugs, thereby rendering anti-cancer treatments less efficient[8,31,34,57]. Therefore, the protective effect of the NIH/3T3-derived matrix on the 4T1 tumor cell viability was evaluated using an additional toxicity test. In this assay we included 4T1 cells that were stably transfected with luciferase. By measuring the luciferase expression we were able to selectively evaluate the viability of 4T1 tumor cells in mono- and cospheroids, 72h after treatment (figure 11). The results obtained on spheroids treated with DOX-liposomes alone and DOX-liposomes coadministered with microbubbles and exposed to ultrasound indicate that 4T1 cells in the cospheroids were less efficiently killed. This confirms that NIH/3T3 fibroblasts can indeed protect the tumor cells from doxorubicin. However, upon treating the spheroids with both types of DOX-liposome-loaded microbubbles and ultrasound, the treatment was equally effective in killing the tumor cells in mono- and cospheroids. Similar to the results in figure 9, the DOX-liposome-loaded microbubbles resulted in an overall stronger reduction of tumor cell viability than the control samples and were equally effective as free doxorubicin.

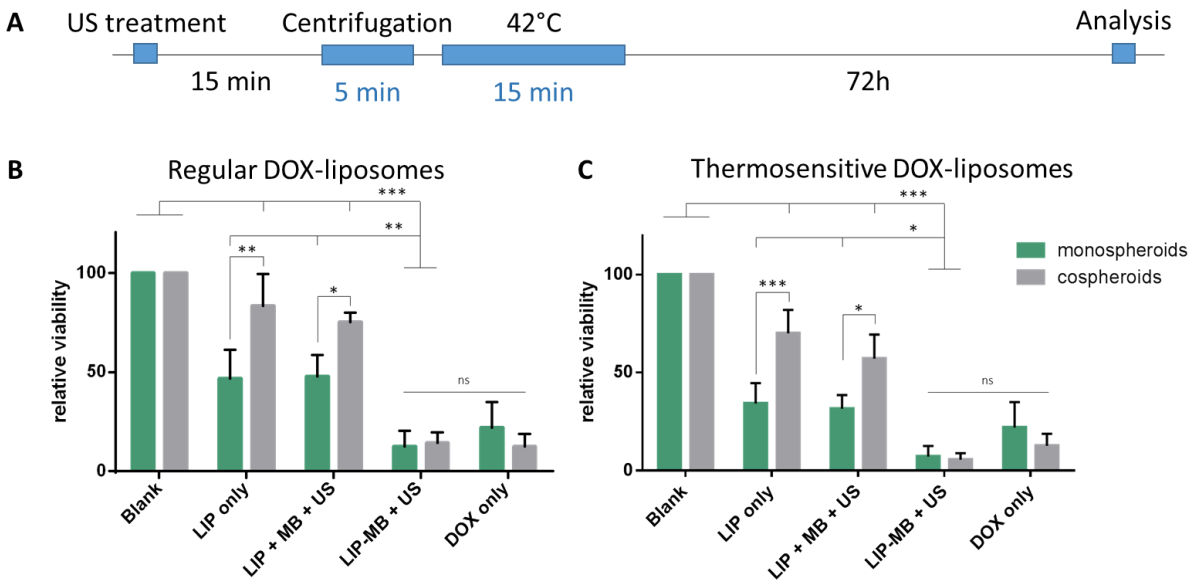

Figure 11: **Selective viability of 4T1 tumor cells 72h after treatment. (A)** Time diagram: 15 min after ultrasound treatment, the spheroids were centrifuged to remove any remaining free doxorubicin or DOX-liposomes. Subsequently, the spheroids were exposed to 42°C for 15 min. After 72h, the viability of the luciferase positive tumor cells was analyzed using a Luciferase-based viability assay. Tumor cell viability after treatment with **(B)** regular DOX-liposome samples and **(C)** thermosensitive DOX-liposome samples. DOX = doxorubicin; LIP = DOX-liposomes; MB = microbubbles; US = ultrasound; LIP + MB + US = DOX-liposomes and microbubbles coadministered before ultrasound radiation; LIP-MB + US = DOX-liposomes loaded onto the microbubbles and exposed to ultrasound, i.e. sonoprinting. Significance levels are determined using a Bonferroni multiple comparison test: ns for $P>0.05$, * for $P<0.05$, ** for $P<0.01$, *** for $P<0.001$.

Discussion

In this study, we found that treatment of free-floating spheroids with nanoparticle-loaded microbubbles and ultrasound results in the superficial deposition of the nanoparticles on the spheroid surface (figure 5&6). The patches closely resemble the sonoprinted patches that we observed before in 2D cell cultures[25]. Both inert polystyrene beads (which cannot leak any fluorophore) and liposomes could be sonoprinted onto the tumor spheroids, as seen in figure 5, indicating that the liposomes remained intact and that the treatment did not result in liposomal fragmentation or leaching of the liposomal dye. This is supported by the findings of Luan et al.[58], who showed that intact liposomes are released from the microbubble shell upon microbubble cavitation.

Our results furthermore show that nanoparticle delivery is limited to the outer cell layers of the spheroids (figure 6), which can be explained by the fact that sonoprinting occurs following a direct interaction between nanoparticle-loaded microbubbles and cells, as schematically presented in figure 1)[26]. In addition, the fact that the deposition of the nanoparticles remains restricted to the surface of the spheroids is supported by earlier findings that show limited penetration of liposomes in tissues (maximally 40-50 µm from the nearest blood vessel), depending on their size and charge[7,59–62]. Moreover, we have previously shown that upon release from the microbubbles, the nanoparticles remain (party) attached to fragments of the microbubble shell[26], possibly leading to clusters of nanoparticles that might contribute to the restricted penetration as well.

Although nanoparticle penetration in the spheroids remained restricted, we observed that the nanoparticle patches can serve as a local reservoir from where drugs can be released and, finally, reach deeper lying cells (figure 7). Since the regular DOX-liposomes showed little doxorubicin leakage after 24h (figure 7D&E), we employed thermosensitive liposomes to induce rapid doxorubicin release (figure 7H&I). In this way, we confirmed that doxorubicin released from sonoprinted liposomal patches was able to penetrate deeper into the tissue to eventually reach the nuclei of cells all the way to the center of the spheroid.

It seems counterintuitive that a comparable cytotoxicity was achieved when spheroids were treated with microbubbles carrying either regular DOX-liposomes or thermosensitive DOX-liposomes (figure 9 and 11). Especially as doxorubicin remained encapsulated in the regular DOX-liposomes (at least at 24h after treatment) while it was immediately released from the thermosensitive DOX-liposomes upon short heating (figure 7). However, both the spheroid morphology (figure 8) and the doxorubicin leakage after 48h (figure 10) suggest that the cytotoxic effects by regular DOX-liposomes occur at a later time compared to thermosensitive DOX-liposomes, indicating that doxorubicin was eventually able to leak out of regular DOX-liposomes and lead to equal cell killing after 72h. The mechanisms

which govern release of doxorubicin from Doxil® (being comparable to the regular DOX-liposomes in this study) are not yet fully elucidated[51,63,64]. Doxil® liposomes have been reported to leak doxorubicin extremely slowly *in vitro*[42,53], which does not seem to explain their effect *in vivo*. Regarding the release *in vivo*, it has been suggested that the uptake of Doxil® liposomes by a selected population of tumor cells and/or macrophages might result in apoptosis of these cells and a subsequent release of the remaining free doxorubicin present in their cytosol[42,53,63]. Another hypothesis is that, since doxorubicin is encapsulated in the liposomes through remote loading in the presence of ammonium sulfate or similar, an enhanced ammonia concentration at the tumor site (through an activation of the glutaminolysis pathway) may reverse the encapsulation process and result in a rapid release of the doxorubicin[51]. Whether or not these mechanisms play a role in tumor spheroids in this study, remains an open question.

Even though mono- and cospheroids vary significantly in composition, only minor differences in penetration of liposomes and doxorubicin were found (figure 7 and supplementary figure 1). Since DOX-liposomes were not able to infiltrate monospheroids, it comes as no surprise that they were unable to infiltrate cospheroids either, as inclusion of fibroblasts makes the penetration barrier even stronger[7,34,65]. However, free doxorubicin easily penetrated both mono- and cospheroids, in contrast to earlier reports, where limited penetration of doxorubicin in spheroids with high stromal content was observed[55,56]. Possibly the rather small size of the spheroids used in this study, allowed doxorubicin to penetrate throughout the entire spheroid volume, regardless of the stromal content. Also, larger spheroids can develop an acidic core, due to insufficient removal of waste products. This lower pH can protect the cells from weak acid drugs such as mitoxantrone and anthracyclines[32], an effect that is most likely not present in the tumor spheroids used in this study. Nevertheless, the selective toxicity assay (figure 11) revealed the pro-carcinogenic effect of cancer-associated fibroblasts in our spheroids, as DOX-liposomes alone and DOX-liposomes coadministered with microbubbles and exposed to ultrasound were more effective in mono- than in cospheroids. Yet, loading DOX-liposomes onto microbubbles resulted in a stronger killing of the 4T1 tumor cells in both mono- and cospheroids.

While tumor spheroids have a higher cellular complexity than monolayer cultures and are therefore a better representative of the *in vivo* situation, there are evidently some limitations to their predictability as well. Since microbubbles are too large to extravasate, they will remain inside the vascular compartment *in vivo*. As a result, the presence of both blood flow and an endothelial cell layer would normally permit only a brief and indirect contact between the target tissue and the drug-carrying microbubbles. However, when using targeted microbubbles, it is possible to locally induce accumulation of the microbubbles and extend the contact time, to resemble the conditions present in this study. Targeting can be achieved through the incorporation of tumor vasculature-specific ligands,

like cyclic RGD or E-selectin, on the microbubble shell[66–68], as well as through physical forces such as the application of an external magnetic field[69,70] or ultrasound-induced radiation forces[71–73]. Adding targeting moieties to the liposomes could also affect the liposomal uptake through receptor-mediated internalization[74]. Secondly, the lack of an endothelial cell layer in this spheroid model makes it impossible to evaluate the impact of this barrier in the current study. Nevertheless, it has been extensively shown that ultrasound-driven microbubbles can lead to the disruption of the vascular wall through the formation of pores in the endothelial cell membranes and the opening of gap junctions,[62,75,76] as notably exemplified for the highly impermeable vascular wall that makes up the blood-brain-barrier[77,78]. However, unlike in brain parenchyma, where any cell is within 2 or 3 cells away from a blood vessel[77], peripheral tumors can form avascular regions where viable cells can be as far as 200 µm away from the nearest capillaries[79,80]. An efficient treatment of such tissues requires a therapy that can overcome the enhanced stromal barrier and can reach the deeper laying layers. Therefore, 3D multicellular models remain suitable models for *in vitro* evaluation of tumor treatment strategies.

Future studies could be performed on more advanced 3D cultures, to obtain a better understanding and predictability of ultrasound-mediated therapeutic applications. For example, tumor spheroids encompassing blood vessel-like structures can provide a better representation of the vascular barrier [81,82]. Alternatively, tumor spheroids grown in microfluidic chips could be employed as they mimic the blood flow around the tissue more accurately[83,84]. However, it is important to remember that confined spaces and rigid membranes yield acoustic artefacts, limiting the use of chip-based culture systems for the evaluation of ultrasound-mediated therapeutic applications.

While this study focused on understanding the mechanisms of sonoprinting in soft tissues, we envision that apart from the delivery of chemotherapeutics with a poor risk-benefit ratio, sonoprinting might be beneficial to several localized therapies *in vivo*. Due to the superficial nature of the observed effects, it can be expected that only targets within and directly around the bloodstream can be reached. However this opens up possibilities for those applications that can benefit from endothelial drug delivery. Examples in this context are the local treatment of bacterial biofilms and atherosclerotic plaques. In earlier work we have demonstrated that sonoprinting using microbubbles loaded with genetic drugs (pDNA, mRNA) can also result in high gene expression levels[40,85], which could be useful to alter the tumor microenvironment by means of cancer immunotherapy. To allow the *in vivo* translation of sonoprinting for tumor therapy, the microbubble loading capacity needs to be sufficient to achieve the desired drug dose. A single injection of Doxil® liposomes is administered to patients in a concentration ranging from 20-50 mg doxorubicin/m², depending on the indication. This corresponds to 34-85 mg doxorubicin for a regular adult patient. Since we calculated that on average 1.6×10^{-7}µg doxorubicin is loaded onto one microbubble, approx. 10^{11} of these microbubbles should be

administered to the patient to attain a similar drug dose. The recommended dose of the clinically approved contrast agent Definity® equals 10^{10} microbubbles for a regular adult patient[24]. However, it has been demonstrated that a 1000 times higher Definity® dose is well-tolerated in primates[86,87]. Following these considerations, we assume that clinically approved microbubble doses may be suitable to administer a sufficient doxorubicin dose. Moreover, as we were able to significantly improve the cytotoxic effects on spheroid cells by loading the DOX-liposomes onto the microbubbles compared to DOX-liposomes alone (figure 9 and 11), we hypothesize that the doxorubicin concentration administered to the patient could be reduced, while maintaining clinical effects.

While in this work thermosensitive liposomes were primarily used to study the fate of the released doxorubicin from the DOX-liposome patches, the use of ThermoDOX® for ultrasound-triggered treatments holds great potential as well. ThermoDOX® liposomes combined with high intensity focused ultrasound (HIFU) are currently clinically evaluated[88], since a local hyperthermia to release the drugs can be induced by ultrasound at the appropriate radiation parameters. As such, we could envision a treatment protocol where a set of ultrasound pulses would be successively applied to allow a local drug delivery by sonoprinting, thereby increasing the drug dose at the target site, followed by a release of the drugs into the target tissue.

Conclusion

In this study we have demonstrated that nanoparticle-loaded microbubbles exposed to ultrasound can locally deposit the nanoparticles onto the outer layers of 3D mono- and cospheroids. This ultrasound-triggered delivery can be attributed to sonoprinting, which only occurs when nanoparticles are loaded onto the microbubble surface. We showed that doxorubicin-loaded liposomes could be successfully sonoprinted on the surface of tumor spheroids. Following sonoprinting, doxorubicin was released from the superficial liposomal patches, penetrated in the spheroids and exerted its cytotoxic effect. In summary, sonoprinting holds great promise to improve the intratumoral delivery of chemotherapeutics whose use is often limited by off-target effects. Future work will therefore focus on exploring its potential for *in vivo* drug delivery.

Acknowledgements

S. Roovers is a doctoral fellow of the Special Research Fund in Flanders Belgium (BOF-Vlaanderen). The project was also funded through NanoCOMIT, an SBO project granted by the Institute for the Promotion of Innovation through Science and Technology in Flanders, Belgium (IWT-Vlaanderen, project number 140061). The support of all of these institutes is gratefully acknowledged. We also thank L. Pieters for her indispensable technical contribution.

Supplementary data

Supplementary Table 1: average size and PdI of different liposomes, as determined by DLS.

	AVERAGE SIZE (NM)	PDI
REGULAR + DID	119	0,316
REGULAR + DOX	199	0,189
REGULAR + DOX + DID	210	0,238
THERMO + DOX	202	0,326
THERMO + DOX + DID	214	0,314

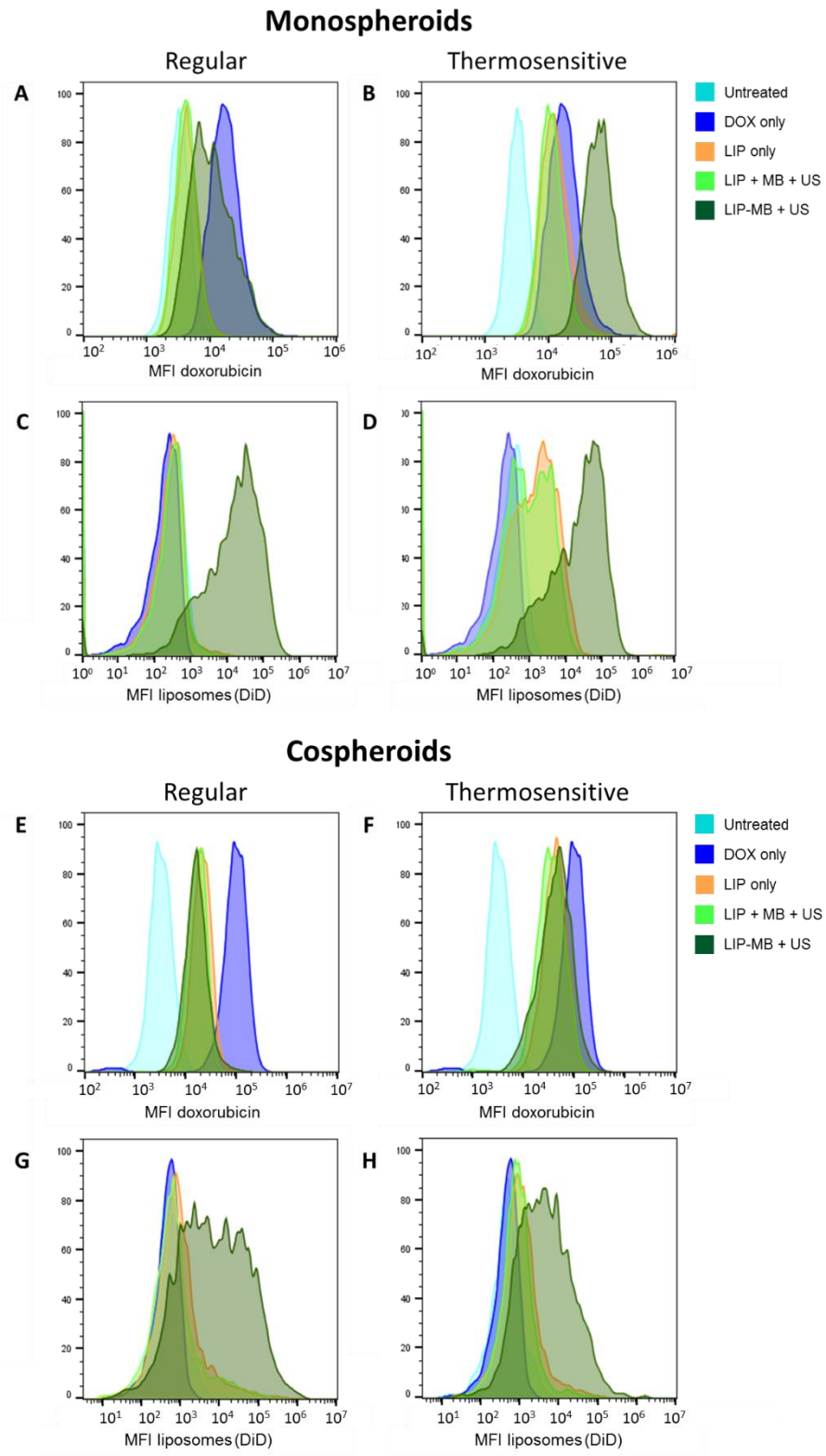

Supplementary Figure 1: Histograms corresponding to flow intensity scatter plots represented in figure 7. Doxorubicin fluorescence after treatment with **(A-E)** regular and **(B-F)** thermosensitive liposomes in **(A-B)** monospheroids and **(E-F)** cospheroids, and liposomal fluorescence after treatment with **(C-G)** regular and **(D-H)** thermosensitive liposomes in **(C-D)** monospheroids and **(G-H)** cospheroids DOX = doxorubicin; LIP = DOX-liposomes; MB = microbubbles; US = ultrasound; LIP + MB + US = DOX-liposomes and microbubbles coadministered before ultrasound radiation; LIP-MB + US = DOX-liposomes loaded onto the microbubbles and exposed to ultrasound (i.e. sonoprinting).

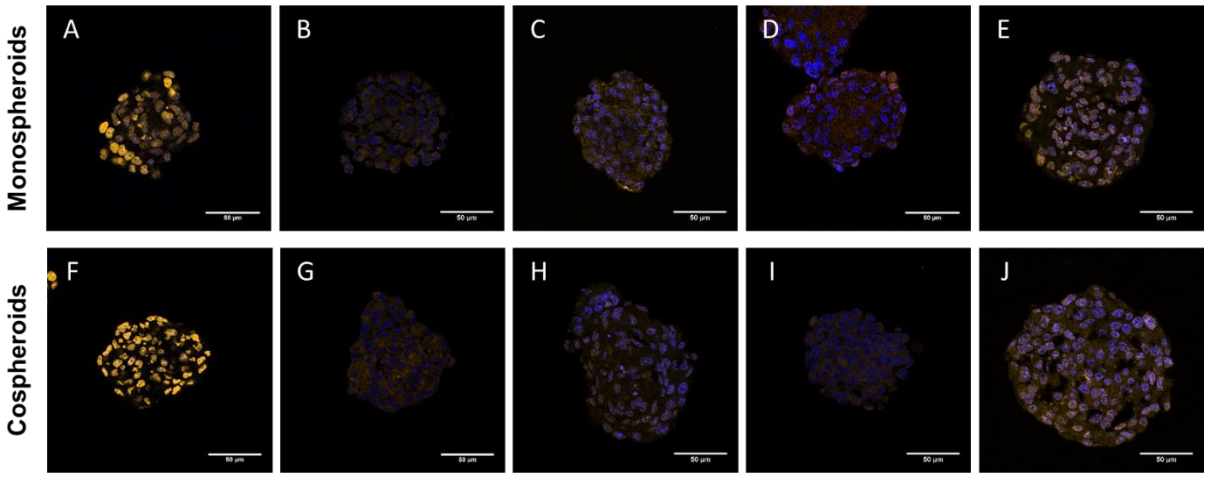

Supplementary Figure 2: Confocal images of 10 µm cryosections of **(A-E)** monospheroids and **(F-J)** cospheroids treated with controls: **(A&F)** DOX only; **(B&G)** regular or **(C&H)** thermosensitive DOX-liposomes only; **(D&I)** regular or **(E&J)** thermosensitive DOX-liposomes coadministered with microbubbles and exposed to ultrasound. Blue = DAPI, orange = doxorubicin, red = liposomes (DiD). The scale bar indicates 50 µm.

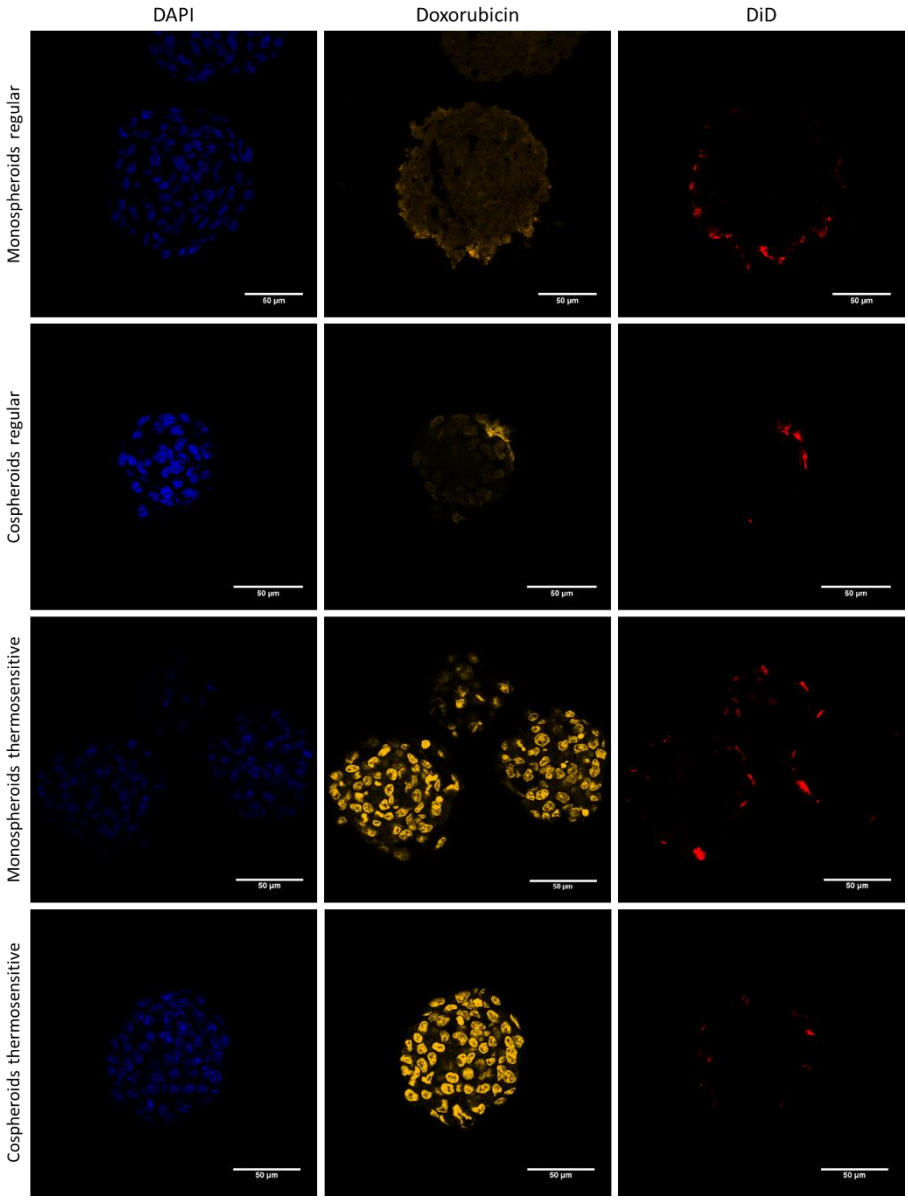

Supplementary Figure 3: Individual fluorescence channels of confocal images depicted in figure 7D,E,H,I. From left to right: DAPI fluorescence, doxorubicin fluorescence and DiD fluorescence. The scale bar indicates 50 µm.

References

1. Maeda, H. Macromolecular Therapeutics in Cancer Treatment: The EPR Effect and Beyond. *Journal of Controlled Release*. 2012, pp 138–144.

2. Lammers, T.; Kiessling, F.; Hennink, W. E.; Storm, G. Drug Targeting to Tumors: Principles, Pitfalls and (Pre-) Clinical Progress. *Journal of Controlled Release*. 2012, pp 175–187.

3. Dreher, M. R.; Liu, W.; Michelich, C. R.; Dewhirst, M. W.; Yuan, F.; Chilkoti, A. Tumor Vascular Permeability, Accumulation, and Penetration of Macromolecular Drug Carriers. *J. Natl. Cancer Inst.* **2006**, *98*, 335–344.

4. Maeda, H. Toward a Full Understanding of the EPR Effect in Primary and Metastatic Tumors as Well as Issues Related to Its Heterogeneity. *Advanced Drug Delivery Reviews*. 2015, pp 3–6.

5. Junttila, M. R.; De Sauvage, F. J. Influence of Tumour Micro-Environment Heterogeneity on Therapeutic Response. *Nature*. 2013, pp 346–354.

6. Wilhelm, S.; Tavares, A. J.; Dai, Q.; Ohta, S.; Audet, J.; Dvorak, H. F.; Chan, W. C. W. Analysis of Nanoparticle Delivery to Tumours. *Nat. Rev. Mater.* **2016**, *1*, 16014.

7. Priwitaningrum, D. L.; Blondé, J. B. G.; Sridhar, A.; van Baarlen, J.; Hennink, W. E.; Storm, G.; Le Gac, S.; Prakash, J. Tumor Stroma-Containing 3D Spheroid Arrays: A Tool to Study Nanoparticle Penetration. *J. Control. Release* **2016**, *244*, 257–268.

8. Prakash, J.; Pinzani, M. Fibroblasts and Extracellular Matrix: Targeting and Therapeutic Tools in Fibrosis and Cancer. *Advanced Drug Delivery Reviews*. 2017, pp 1–2.

9. Boissenot, T.; Bordat, A.; Fattal, E.; Tsapis, N. Ultrasound-Triggered Drug Delivery for Cancer Treatment Using Drug Delivery Systems: From Theoretical Considerations to Practical Applications. *Journal of Controlled Release*. 2016.

10. Wilhelm, S.; Tavares, A. J.; Dai, Q.; Ohta, S.; Audet, J.; Dvorak, H. F.; Chan, W. C. W. Analysis of Nanoparticle Delivery to Tumours. *Nature Reviews Materials*. 2016.

11. Sahle, F. F.; Gulfam, M.; Lowe, T. L. Design Strategies for Physical-Stimuli-Responsive Programmable Nanotherapeutics. *Drug Discov. Today* **2018**, *23*, 992–1006.

12. Gulfam, M.; Sahle, F. F.; Lowe, T. L. Design Strategies for Chemical-Stimuli-Responsive Programmable Nanotherapeutics. *Drug Discovery Today*. 2019.

13. Stewart, M. P.; Langer, R.; Jensen, K. F. Intracellular Delivery by Membrane Disruption: Mechanisms, Strategies, and Concepts. *Chemical Reviews*. 2018, pp 7409–7531.

14. Hernot, S.; Klibanov, A. L. Microbubbles in Ultrasound-Triggered Drug and Gene Delivery. *Advanced Drug Delivery Reviews*. 2008, pp 1153–1166.

15. Roovers, S.; Segers, T.; Lajoinie, G.; Deprez, J.; Versluis, M.; De Smedt, S. C.; Lentacker, I. The Role of Ultrasound-Driven Microbubble Dynamics in Drug Delivery: From Microbubble Fundamentals to Clinical Translation. *Langmuir* **2019**, acs.langmuir.8b03779.

16. Lentacker, I.; De Cock, I.; Deckers, R.; De Smedt, S. C.; Moonen, C. T. W. Understanding Ultrasound Induced Sonoporation: Definitions and Underlying Mechanisms. *Advanced Drug Delivery Reviews*. 2014, pp 49–64.

17. Kooiman, K.; Vos, H. J.; Versluis, M.; De Jong, N. Acoustic Behavior of Microbubbles and Implications for Drug Delivery. *Advanced Drug Delivery Reviews*. 2014.

18. De Cock, I.; Zagato, E.; Braeckmans, K.; Luan, Y.; de Jong, N.; De Smedt, S. C.; Lentacker, I. Ultrasound and Microbubble Mediated Drug Delivery: Acoustic Pressure as Determinant for Uptake via Membrane Pores or Endocytosis. *J. Control. Release* **2015**, *197*.

19. Helfield, B.; Chen, X.; Watkins, S. C.; Villanueva, F. S. Biophysical Insight into Mechanisms of Sonoporation. *Proc. Natl. Acad. Sci.* **2016**, *113*.

20. Burke, C. W.; Alexander, E.; Timbie, K.; Kilbanov, A. L.; Price, R. J. Ultrasound-Activated Agents Comprised of 5FU-Bearing Nanoparticles Bonded to Microbubbles Inhibit Solid Tumor Growth and Improve Survival. *Mol. Ther.* **2014**, *22*, 321–328.

21. Burke, C. W.; Hsiang, Y. H. J.; Alexander IV, E.; Kilbanov, A. L.; Price, R. J. Covalently Linking Poly(Lactic-Co-Glycolic Acid) Nanoparticles to Microbubbles before Intravenous Injection Improves Their Ultrasound-Targeted Delivery to Skeletal Muscle. *Small* **2011**, *7*, 1227–1235.

22. Vandenbroucke, R. E.; Lentacker, I.; Demeester, J.; De Smedt, S. C.; Sanders, N. N. Ultrasound Assisted SiRNA Delivery Using PEG-SiPlex Loaded Microbubbles. *J. Control. Release* **2008**, *126*, 265–273.

23. Geers, B.; Lentacker, I.; Sanders, N. N.; Demeester, J.; Meairs, S.; De Smedt, S. C. Self-Assembled Liposome-Loaded Microbubbles: The Missing Link for Safe and Efficient Ultrasound Triggered Drug-Delivery. *J. Control. Release* **2011**, *152*, 249–256.

24. Lentacker, I.; Geers, B.; Demeester, J.; De Smedt, S. C.; Sanders, N. N. Design and Evaluation of Doxorubicin-Containing Microbubbles for Ultrasound-Triggered Doxorubicin Delivery: Cytotoxicity and Mechanisms Involved. *Mol. Ther.* **2010**, *18*, 101–108.

25. De Cock, I.; Lajoinie, G.; Versluis, M.; De Smedt, S. C.; Lentacker, I. Sonoprinting and the Importance of Microbubble Loading for the Ultrasound Mediated Cellular Delivery of Nanoparticles. *Biomaterials* **2016**, *83*, 294–307.

26. De Cock, I. Unravelling Microbubble-Cell Interactions and Drug Delivery Mechanisms in Ultrasound-Guided Therapy, Ghent University, 2016.

27. Vos, H. J.; Dollet, B.; Bosch, J. G.; Versluis, M.; de Jong, N. Nonspherical Vibrations of Microbubbles in Contact with a Wall-A Pilot Study at Low Mechanical Index. *Ultrasound Med. Biol.* **2008**, *34*, 685–688.

28. Lajoinie, G.; Luan, Y.; Gelderblom, E.; Dollet, B.; Lentacker, I.; Dewitte, H.; De Jong, N.; Versluis, M. Non-Spherical Oscillations Drive the Lipid Shedding of Microbubbles near a Boundary.

29. Helfield, B. L.; Leung, B. Y. C.; Goertz, D. E. The Effect of Boundary Proximity on the Response of Individual Ultrasound Contrast Agent Microbubbles. *Phys. Med. Biol.* **2014**, *59*, 1721–1745.

30. Alemany-Ribes, M.; Semino, C. E. Bioengineering 3D Environments for Cancer Models. *Adv. Drug Deliv. Rev.* **2014**, *79*, 40–49.

31. Leong, D. T.; Ng, K. W. Probing the Relevance of 3D Cancer Models in Nanomedicine Research. *Adv. Drug Deliv. Rev.* **2014**, *79*, 95–106.

32. Mehta, G.; Hsiao, A. Y.; Ingram, M.; Luker, G. D.; Takayama, S. Opportunities and Challenges for Use of Tumor Spheroids as Models to Test Drug Delivery and Efficacy. *J. Control. Release* **2012**, *164*, 192–204.

33. Chandrasekaran, S. Gather Round: In Vitro Tumor Spheroids as Improved Models of in Vivo Tumors. *J. Bioeng. Biomed. Sci.* **2012**, *02*.

34. Choi, S. Y. C.; Lin, D.; Gout, P. W.; Collins, C. C.; Xu, Y.; Wang, Y. Lessons from Patient-Derived Xenografts for Better in Vitro Modeling of Human Cancer. *Adv. Drug Deliv. Rev.* **2014**, *79*, 222–237.

35. Xu, X.; Farach-Carson, M. C.; Jia, X. Three-Dimensional in Vitro Tumor Models for Cancer Research and Drug Evaluation. *Biotechnol. Adv.* **2014**, *32*, 1256–1268.

36. Pampaloni, F.; Ansari, N.; Stelzer, E. H. K. High-Resolution Deep Imaging of Live Cellular Spheroids with Light-Sheet-Based Fluorescence Microscopy. *Cell Tissue Res.* **2013**, *352*, 161–177.

37. Vrij, E.; Rouwkema, J.; Lapointe, V.; Van Blitterswijk, C.; Truckenmüller, R.; Rivron, N. Directed Assembly and Development of Material-Free Tissues with Complex Architectures. *Adv. Mater.* **2016**, *28*, 4032–4039.

38. Rivron, N. C.; Vrij, E. J.; Rouwkema, J.; Le Gac, S.; van den Berg, A.; Truckenmuller, R. K.; van Blitterswijk, C. A. Tissue Deformation Spatially Modulates VEGF Signaling and Angiogenesis. *Proc. Natl. Acad. Sci.* **2012**.

39. Carugo, D.; Owen, J.; Crake, C.; Lee, J. Y.; Stride, E. Biologically and Acoustically Compatible Chamber for Studying Ultrasound-Mediated Delivery of Therapeutic Compounds. *Ultrasound Med. Biol.* **2015**, *41*, 1927–1937.

40. De Temmerman, M. L.; Dewitte, H.; Vandenbroucke, R. E.; Lucas, B.; Libert, C.; Demeester, J.; De Smedt, S. C.; Lentacker, I.; Rejman, J. MRNA-Lipoplex Loaded Microbubble Contrast Agents for Ultrasound-Assisted Transfection of Dendritic Cells. *Biomaterials* **2011**, *32*, 9128–9135.

41. van Elk, M.; Ozbakir, B.; Barten-Rijbroek, A. D.; Storm, G.; Nijsen, F.; Hennink, W. E.; Vermonden, T.; Deckers, R. Alginate Microspheres Containing Temperature Sensitive Liposomes (TSL) for MR-Guided Embolization and Triggered Release of Doxorubicin. *PLoS One* **2015**, *10*, e0141626.

42. Barenholz, Y. Doxil® - The First FDA-Approved Nano-Drug: Lessons Learned. *J. Control. Release* **2012**, *160*, 117–134.

43. Zanoni, M.; Piccinini, F.; Arienti, C.; Zamagni, A.; Santi, S.; Polico, R.; Bevilacqua, A.; Tesei, A. 3D Tumor Spheroid Models for in Vitro Therapeutic Screening: A Systematic Approach to Enhance the Biological Relevance of Data Obtained. *Sci. Rep.* **2016**.

44. Foty, R. A.; Steinberg, M. S. The Differential Adhesion Hypothesis: A Direct Evaluation. *Dev. Biol.* **2005**.

45. Lombardo, D.; Calandra, P.; Barreca, D.; Magazù, S.; Kiselev, M. Soft Interaction in Liposome Nanocarriers for Therapeutic Drug Delivery. *Nanomaterials* **2016**.

46. Pattni, B. S.; Chupin, V. V.; Torchilin, V. P. New Developments in Liposomal Drug Delivery. *Chem. Rev.* **2015**.

47. Xing, H.; Hwang, K.; Lu, Y. Recent Developments of Liposomes as Nanocarriers for Theranostic Applications. *Theranostics*. 2016.

48. Centonze, V. E.; White, J. G. Multiphoton Excitation Provides Optical Sections from Deeper

within Scattering Specimens than Confocal Imaging. *Biophys. J.* **1998**.

49. Vinci, M.; Gowan, S.; Boxall, F.; Patterson, L.; Zimmermann, M.; Court, W.; Lomas, C.; Mendiola, M.; Hardisson, D.; Eccles, S. A. Advances in Establishment and Analysis of Three-Dimensional Tumor Spheroid-Based Functional Assays for Target Validation and Drug Evaluation. *BMC Biol.* **2012**.

50. Ruggiero, E.; Alonso-De Castro, S.; Habtemariam, A.; Salassa, L. Upconverting Nanoparticles for the near Infrared Photoactivation of Transition Metal Complexes: New Opportunities and Challenges in Medicinal Inorganic Photochemistry. *Dalt. Trans.* **2016**.

51. Silverman, L.; Barenholz, Y. In Vitro Experiments Showing Enhanced Release of Doxorubicin from Doxil® in the Presence of Ammonia May Explain Drug Release at Tumor Site. *Nanomedicine Nanotechnology, Biol. Med.* **2015**, *11*, 1841–1850.

52. Krishna, R.; Ghiu, G.; Mayer, L. D. Visualization of Bioavailable Liposomal Doxorubicin Using a Non-Perturbing Confocal Imaging Technique. *Histol. Histopathol.* **2001**.

53. Russell, L. M.; Hultz, M.; Searson, P. C. Leakage Kinetics of the Liposomal Chemotherapeutic Agent Doxil: The Role of Dissolution, Protonation, and Passive Transport, and Implications for Mechanism of Action. *J. Control. Release* **2018**, *269*, 171–176.

54. Jiang, W.; Lionberger, R.; Yu, L. X. In Vitro and in Vivo Characterizations of PEGylated Liposomal Doxorubicin. *Bioanalysis*. 2011.

55. Durand, R. E. Chemosensitivity Testing in V79 Spheroids: Drug Delivery and Cellular Microenvironment. *J. Natl. Cancer Inst.* **1986**.

56. Jeong, S. Y.; Lee, J. H.; Shin, Y.; Chung, S.; Kuh, H. J. Co-Culture of Tumor Spheroids and Fibroblasts in a Collagen Matrix-Incorporated Microfluidic Chip Mimics Reciprocal Activation in Solid Tumor Microenvironment. *PLoS One* **2016**.

57. Alemany-Ribes, M.; Semino, C. E. Bioengineering 3D Environments for Cancer Models. *Advanced Drug Delivery Reviews*. 2014, pp 40–49.

58. Luan, Y.; Faez, T.; Gelderblom, E.; Skachkov, I.; Geers, B.; Lentacker, I.; van der Steen, T.; Versluis, M.; de Jong, N. Acoustical Properties of Individual Liposome-Loaded Microbubbles. *Ultrasound Med. Biol.* **2012**, *38*, 2174–2185.

59. Grainger, S. J.; Serna, J. V.; Sunny, S.; Zhou, Y.; Deng, C. X.; El-Sayed, M. E. H. Pulsed Ultrasound Enhances Nanoparticle Penetration into Breast Cancer Spheroids. *Mol. Pharm.*

2010, *7*, 2006–2019.

60. Albanese, A.; Tang, P. S.; Chan, W. C. W. The Effect of Nanoparticle Size, Shape, and Surface Chemistry on Biological Systems. *Annu. Rev. Biomed. Eng.* **2012**, *14*, 1–16.

61. Jain, R. K.; Stylianopoulos, T. Delivering Nanomedicine to Solid Tumors. *Nature Reviews Clinical Oncology*. 2010, pp 653–664.

62. Theek, B.; Baues, M.; Ojha, T.; Möckel, D.; Veettil, S. K.; Steitz, J.; Van Bloois, L.; Storm, G.; Kiessling, F.; Lammers, T. Sonoporation Enhances Liposome Accumulation and Penetration in Tumors with Low EPR. *J. Control. Release* **2016**, *231*, 77–85.

63. Storm, G.; Steerenberg, P. A.; Emmen, F.; van Borssum Waalkes, M.; Crommelin, D. J. A. Release of Doxorubicin from Peritoneal Macrophages Exposed in Vivo to Doxorubicin-Containing Liposomes. *BBA - Gen. Subj.* **1988**, *965*, 136–145.

64. Seynhaeve, A. L. B.; Dicheva, B. M.; Hoving, S.; Koning, G. A.; Ten Hagen, T. L. M. Intact Doxil Is Taken up Intracellularly and Released Doxorubicin Sequesters in the Lysosome: Evaluated by in Vitro/in Vivo Live Cell Imaging. *J. Control. Release* **2013**, *172*, 330–340.

65. Kunz-Schughart, L. A.; Kreutz, M.; Knuechel, R. Multicellular Spheroids: A Three-Dimensional in Vitro Culture System to Study Tumour Biology. *Int. J. Exp. Pathol.* **1998**, *79*, 1–23.

66. Ibsen, S.; Shi, G.; Schutt, C.; Shi, L.; Suico, K. D.; Benchimol, M.; Serra, V.; Simberg, D.; Berns, M.; Esener, S. The Behavior of Lipid Debris Left on Cell Surfaces from Microbubble Based Ultrasound Molecular Imaging. *Ultrasonics* **2014**, *54*, 2090–2098.

67. Leow, R. S.; Wan, J. M. F.; Yu, A. C. H. Membrane Blebbing as a Recovery Manoeuvre in Site-Specific Sonoporation Mediated by Targeted Microbubbles. *J. R. Soc. Interface* **2015**, *12*.

68. van Rooij, T.; Skachkov, I.; Beekers, I.; Lattwein, K. R.; Voorneveld, J. D.; Kokhuis, T. J. A.; Bera, D.; Luan, Y.; van der Steen, A. F. W.; de Jong, N.; et al. Viability of Endothelial Cells after Ultrasound-Mediated Sonoporation: Influence of Targeting, Oscillation, and Displacement of Microbubbles. *J. Control. Release* **2016**, *238*, 197–211.

69. Crake, C.; Victor, M. D. Saint; Owen, J.; Coviello, C.; Collin, J.; Coussios, C. C.; Stride, E. Passive Acoustic Mapping of Magnetic Microbubbles for Cavitation Enhancement and Localization. *Phys. Med. Biol.* **2015**, *60*, 785–806.

70. Lee, J. Y.; Crake, C.; Teo, B.; Carugo, D.; de Saint Victor, M.; Seth, A.; Stride, E. Ultrasound-Enhanced SiRNA Delivery Using Magnetic Nanoparticle-Loaded Chitosan-Deoxycholic Acid

Nanodroplets. *Adv. Healthc. Mater.* **2017**, *6*.

71. Lum, A. F. H.; Borden, M. A.; Dayton, P. A.; Kruse, D. E.; Simon, S. I.; Ferrara, K. W. Ultrasound Radiation Force Enables Targeted Deposition of Model Drug Carriers Loaded on Microbubbles. *J. Control. Release* **2006**, *111*, 128–134.

72. Dayton, P.; Klibanov, A.; Brandenburger, G.; Ferrara, K. Acoustic Radiation Force in Vivo: A Mechanism to Assist Targeting of Microbubbles. *Ultrasound Med. Biol.* **1999**, *25*, 1195–1201.

73. Kaya, M.; Toma, C.; Wang, J.; Grata, M.; Fu, H.; Villanueva, F. S.; Chen, X. Acoustic Radiation Force for Vascular Cell Therapy: In Vitro Validation. *Ultrasound Med. Biol.* **2012**, *38*, 1989–1997.

74. Park, Y. C.; Zhang, C.; Kim, S.; Mohamedi, G.; Beigie, C.; Nagy, J. O.; Holt, R. G.; Cleveland, R. O.; Jeon, N. L.; Wong, J. Y. Microvessels-on-a-Chip to Assess Targeted Ultrasound-Assisted Drug Delivery. *ACS Appl. Mater. Interfaces* **2016**, *8*, 31541–31549.

75. Helfield, B.; Chen, X.; Watkins, S. C.; Villanueva, F. S. Biophysical Insight into Mechanisms of Sonoporation. *Proc. Natl. Acad. Sci.* **2016**, *113*, 9983–9988.

76. Qin, P.; Han, T.; Yu, A. C. H.; Xu, L. Mechanistic Understanding the Bioeffects of Ultrasound-Driven Microbubbles to Enhance Macromolecule Delivery. *Journal of Controlled Release*. 2018.

77. Song, K.-H.; Harvey, B. K.; Borden, M. A. State-of-the-Art of Microbubble-Assisted Blood-Brain Barrier Disruption. *Theranostics* **2018**, *8*, 4393–4408.

78. McDannold, N.; Arvanitis, C. D.; Vykhodtseva, N.; Livingstone, M. S. Temporary Disruption of the Blood-Brain Barrier by Use of Ultrasound and Microbubbles: Safety and Efficacy Evaluation in Rhesus Macaques. *Cancer Res.* **2012**, *72*, 3652–3663.

79. Rouwkema, J.; Koopman, B. F. J. M.; Blitterswijk, C. A. V.; Dhert, W. J. A.; Malda, J. Supply of Nutrients to Cells in Engineered Tissues. *Biotechnol. Genet. Eng. Rev.* **2009**, *26*, 163–178.

80. Forster, J.; Harriss-Phillips, W.; Douglass, M.; Bezak, E. A Review of the Development of Tumor Vasculature and Its Effects on the Tumor Microenvironment. *Hypoxia* **2017**, *Volume 5*, 21–32.

81. De Moor, L.; Merovci, I.; Baetens, S.; Verstraeten, J.; Kowalska, P.; Krysko, D. V.; De Vos, W. H.; Declercq, H. High-Throughput Fabrication of Vascularized Spheroids for Bioprinting. *Biofabrication* **2018**, *10*.

82. Hasan, A.; Paul, A.; Vrana, N. E.; Zhao, X.; Memic, A.; Hwang, Y. S.; Dokmeci, M. R.;

Khademhosseini, A. Microfluidic Techniques for Development of 3D Vascularized Tissue. *Biomaterials*. 2014, pp 7308–7325.

83. Albanese, A.; Lam, A. K.; Sykes, E. A.; Rocheleau, J. V.; Chan, W. C. W. Tumour-on-a-Chip Provides an Optical Window into Nanoparticle Tissue Transport. *Nat. Commun.* **2013**, *4*.

84. Ozcelikkale, A.; Moon, H. R.; Linnes, M.; Han, B. In Vitro Microfluidic Models of Tumor Microenvironment to Screen Transport of Drugs and Nanoparticles. *Wiley Interdisciplinary Reviews: Nanomedicine and Nanobiotechnology*. 2017.

85. Lentacker, I.; De Smedt, S. C.; Demeester, J.; Van Marck, V.; Bracke, M.; Sanders, N. N. Lipoplex-Loaded Microbubbles for Gene Delivery: A Trojan Horse Controlled by Ultrasound. *Adv. Funct. Mater.* **2007**.

86. Karshafian, R.; Bevan, P. D.; Williams, R.; Samac, S.; Burns, P. N. Sonoporation by Ultrasound-Activated Microbubble Contrast Agents: Effect of Acoustic Exposure Parameters on Cell Membrane Permeability and Cell Viability. *Ultrasound Med. Biol.* **2009**, *35*, 847–860.

87. Unger, E. C.; Porter, T.; Culp, W.; Labell, R.; Matsunaga, T.; Zutshi, R. Therapeutic Applications of Lipid-Coated Microbubbles. *Adv. Drug Deliv. Rev.* **2004**.

88. Lyon, P. C.; Griffiths, L. F.; Lee, J.; Chung, D.; Carlisle, R.; Wu, F.; Middleton, M. R.; Gleeson, F. V.; Coussios, C. C. Clinical Trial Protocol for TARDOX: A Phase I Study to Investigate the Feasibility of Targeted Release of Lyso-Thermosensitive Liposomal Doxorubicin (ThermoDox®) Using Focused Ultrasound in Patients with Liver Tumours. *J. Ther. Ultrasound* **2017**.